Climbing to the top of Mount Fuji: Uniting theory and observations of oxygen triple isotope systematics

Laurence Y. Yeung
Department of Earth, Environmental and Planetary Sciences
Rice University
Houston, TX 77005, U.S.A.
lyeung@rice.edu

Justin A. Hayles
Jacobs-JETS, Astromaterials Research and Exploration Science, Johnson Space Center
National Aeronautics and Space Administration
Houston, TX 77058, U.S.A.
justin.a.hayles@nasa.gov

INTRODUCTION

The near-simultaneous discovery of both minor isotopes of oxygen in 1929 was a watershed moment for modern science, to say nothing of its impacts on isotope geochemistry. At the time, oxygen was the international standard for atomic weight, as it had been for over twenty-five years. However, chemists and physicists had grown fond of different definitions: physicists used the weight of the ^{16}O atom, while chemists used half the weight of atmospheric oxygen (O_2) to define the precise weight of 16 atomic mass units. While they usually avoided direct conflicts, these contrasting definitions found an unexpected impasse in the near-infrared absorption spectrum of atmospheric oxygen: it contained a series of faint lines that could not be explained by any known atmospheric constituents (Dieke and Babcock 1927; Mulliken 1928).

The key breakthrough came when Herrick Johnston and William Giauque, who were separately studying the thermodynamics of oxygen, realized that small amounts of heavier oxygen isotopes in O_2, ^{17}O and ^{18}O, could generate those weak absorptions. With no prior precedent for these isotopes, Johnston and Giauque relied on the theoretical mass dependence of vibrational frequencies and spectroscopic selection rules from quantum mechanics—then still a young theory—to predict where $^{16}O^{18}O$ and $^{16}O^{17}O$ would absorb. Their predictions were quantitative and definitive (Giauque and Johnston 1929a; b). Together with subsequent observations by Malcolm Dole, George Lane and others (Dole 1935; Dole and Jenks 1944; Dole et al. 1947; Epstein and Mayeda 1953; Lane and Dole 1956)—the discovery of ^{17}O and ^{18}O led the International Union of Pure and Applied Chemistry to redefine atomic weight relative to carbon-12 in 1962, which is still valid today.

Oxygen triple-isotope geochemistry owes its existence to this discovery, which was borne out of a clever application of theory to a puzzling observation. Isotope geochemists today still

rely on theory to fill this same role: to predict and explain observations of nature, using that nexus to make fundamental advances of broader scientific relevance. However, the targets have evolved; our ability to measure variations in oxygen-isotope abundances in natural materials has been transformed by high-precision isotope ratio mass spectrometry and innovative analytical techniques (Nier 1947; McCrea 1950; Sharp 1990; Baker et al. 2002), which have improved in the past few decades to yield parts-per-million (ppm) levels of precision in oxygen-isotope ratios for a wide variety of natural materials (Luz et al. 1999; Luz and Barkan 2000; Barkan and Luz 2005; Pack et al. 2013; Pack and Herwartz 2014b). Concurrently, the explosive growth of computing power, particularly the recent advances in parallel computing, have made first-principles electronic structure calculations more accessible than ever to the geochemist: large chemical systems once considered intractable are being studied routinely *in silico*. How well can theory and observations work together toward new insights in these much more exacting times?

Oxygen triple-isotope geochemistry focuses in two general areas, both of which have been informed and advanced by theory. The mass-independent isotopic fractionation of oxygen preserved in early solar-system condensates (Clayton et al. 1973) and atmospheric ozone (Mauersberger 1981; Thiemens and Heidenreich 1983) stimulated a new wave of theoretical work in the 1990s and 2000s to understand the physical-chemical origins of those anomalies, leading to the discovery of other mass-independent isotope fractionation mechanisms for oxygen and other elements (Röckmann et al. 1998; Hathorn and Marcus 1999; 2000; Farquhar et al. 2001; Gao and Marcus 2001; Clayton 2002; Babikov et al. 2003; Marcus 2004; Schinke et al. 2006; Bergquist and Blum 2007). These signals have led to fundamental discoveries about the formation and evolution of the solar system, Earth history, and biogeochemical cycling (Thiemens 2006). Other chapters in this volume will cover those developments, so we will focus here on the second major area of oxygen triple-isotope geochemistry, that of natural variations in mass-dependent fractionation.

The role of theory in this area is clear: it provides independent, physics-based reference points for oxygen triple-isotope partitioning. Such reference points are invaluable because of the myriad ways in which oxygen isotopes can be fractionated, transported, and mixed to yield the parts-per-million (ppm) level variability that is routinely observed and interpreted (Juranek and Quay 2013; Herwartz et al. 2014; Luz et al. 2014; Young et al. 2016; Bindeman et al. 2018; Sharp et al. 2018); theory can help distinguish the signal from the noise. Theoretical reference points can also lead to analytical innovations and the characterization of unusual processes (Richet et al. 1977; Thiemens 2006; Eiler 2007; Bao et al. 2015; Hayles et al. 2017). Even when imperfect, a theoretical prediction constitutes a vital third approach to high-precision isotope geochemistry that has a different set of biases from experiments and observations.

Are current theoretical methods sufficiently accurate to benchmark oxygen triple-isotope geochemistry? Analogous investigations in the clumped-isotope community (Wang et al. 2004; Schauble et al. 2006b; Guo et al. 2009; Piasecki et al. 2016; Piasecki et al. 2018) suggest that they are not far off: robust features of isotope partitioning have been observed across theory, experiment, and observations to within several tens of ppm. Some disagreements in isotopic fractionation factors have persisted, however [e.g., for acid digestion fractionation (Guo et al. 2009; Murray et al. 2016; Müller et al. 2017; Petersen et al. 2019; Swart et al. 2019; Zhang et al. 2020)], resulting in barriers to reproducibility and (in our view) limits to the certainty with which isotopic records can be interpreted. Breaking through these barriers to find agreement at the

single-digit ppm level would be both a triumph for theoretical approaches and transformative for oxygen triple-isotope geochemistry. This article aims to evaluate how close the state of the art is to this target, and hopefully to guide the way forward.

In this article, we will first cover basic concepts and notation relevant to oxygen triple-isotope geochemistry. Second, we will examine what theory predicts for oxygen triple-isotope variability in chemical processes. Third, we will examine the systematic biases that may be present in theoretical approaches, with special attention paid to first-principles electronic structure calculations. Fourth, we will consider the current limits of analytical accuracy and the complications introduced by physical effects in real systems. Finally, we will revisit the triple-isotope mass dependence of carbonate acid digestion as a case study of how theory and experiment can work together to improve both each other and ultimately also our understanding of a process that is vital for the emerging area of carbonate-based paleohydrology.

BASIC CONCEPTS

The equations

Molecules as physical entities can be viewed as collections of balls and springs, with the balls being nuclei of atoms and the springs being the bonds that tie them together. The strength of chemical bonds is tied primarily to electrons, which are each about 1/30,000th the mass of an oxygen atom. Consequently, changing the mass of an oxygen atom has little effect on basic molecular structure or chemistry in most cases. However, exchanging an oxygen atom for a heavier isotope will change the frequencies at which a molecule naturally oscillates: heavier masses connected to the same springs will yield lower frequencies of vibration. It is these subtle variations in vibrational frequencies in isotopically substituted molecules, which have subtle effects on molecular enthalpy and entropy, that drive a majority of chemical isotope effects.

Bigeleisen, Goeppert-Mayer, and Urey are credited with deriving expressions describing the thermodynamics of isotopically substituted gas-phase molecules (Bigeleisen and Goeppert-Mayer 1947; Urey 1947). They used the reduced partition function ratio β^* between two isotopic variants of molecules as a building block to describe isotope-exchange reactions:

$$\beta^{i} = \prod_{i=1}^{3N-6} \left(\frac{\nu_i^{i}}{\nu_i} \right)_{MMI} \left(\frac{e^{-U_i^{i}/2}}{e^{-U_i/2}} \right)_{ZPE} \left(\frac{1-e^{-U_i}}{1-e^{-U_i^{i}}} \right)_{EXC} \quad (1)$$

Here, ν_i is the ith harmonic vibrational frequency of the molecule (of $3N-6$ total for polyatomic molecules, $3N-5$ for diatomics), $U_i = h\nu_i/k_B T$ (or $hc\nu_i/k_B T$ if ν_i is expressed in wavenumbers), N is the number of atoms in the molecule, h is Planck's constant, k_B is Boltzmann's constant, and T is the temperature. This equation represents the thermodynamic preference to form an isotopically substituted molecule (denoted above by an asterisk) compared to the isotopically "normal" molecule, in an idealized equilibrium between these species and free atoms (e.g., O atoms in the case of oxygen triple isotopes). We note that the definition of β^* includes effects due to changes in molecular symmetry upon isotopic substitution, so symmetry numbers are absent from the right-hand side of eqn. (1).

The equilibrium isotopic fractionation between species A and species B in the reaction A + B^* ⇌ A^* + B, in which a single isotope is exchanged, is thus written as

$$ {}^{18}_{\square}\alpha_{A-B} = \frac{{}^{18}_{\square}\beta_A^{i}}{{}^{18}_{\square}\beta_B^{i}} = \frac{\left[\dfrac{\left({}^{18}_{\square}O/{}^{16}_{\square}O\right)_A}{\left({}^{18}_{\square}O/{}^{16}_{\square}O\right)_{atomic}}\right]}{\left[\dfrac{\left({}^{18}_{\square}O/{}^{16}_{\square}O\right)_B}{\left({}^{18}_{\square}O/{}^{16}_{\square}O\right)_{atomic}}\right]} \quad (2) $$

Many excellent discussions of eqn. (1) exist (Schauble 2004; Liu et al. 2010), so we will highlight only a few elements most germane to this discussion. First, the expression has inherent assumptions: it is derived assuming that bonds are perfect springs holding atoms together (the so-called harmonic oscillator approximation) and that bond lengths are constant (the so-called rigid-rotor approximation). Clearly, these two approximations cannot simultaneously be true, but they simplify the math considerably, and are good approximations of many real systems at Earth-surface temperatures. Moreover, the approximations allow one to separate the energies associated with molecular vibrations (*ZPE* and *EXC* subscripts) from those involving translations and rotations (*MMI* subscript). The *ZPE* (zero-point energy) term corresponds to the ratio of "occupancies" of the lowest-energy vibrational states v_0 and v_0^*, i.e., how often an isotopically substituted molecule would be in that state compared to its unsubstituted counterpart at a given temperature. The *EXC* term corresponds to the occupancies of the higher vibrational states. The *MMI* term is deceptively simple because it relates the ratio of masses and moments of inertia of the molecule (from classical mechanics) to a ratio of vibrational frequencies (from quantum mechanics) through the Teller-Redlich isotopic product rule (Redlich 1935). Indeed, without the harmonic-oscillator and rigid-rotor approximations, eqn. (1) would be much more complicated. There are many notable instances in which these approximations are insufficient for describing isotope fractionation; we will return to these later.

In liquids, solutions, and solids—which are in many cases the phases most relevant to oxygen triple isotopes—the potential range of atom-atom interactions broadens considerably compared to an isolated gas-phase molecule. Oxygen atoms in aqueous oxides (e.g., HCO_3^- SO_4^{2-}, and H_4SiO_4) interact meaningfully with the solvent, so one expects aqueous isotopic fractionation of oxygen to depend on the strength and number of these interactions; in other words, in addition to influences on vibrations of the solute, there are simply more relevant vibrational modes *i* to consider in eqn. (1), and the "sphere of influence" of an isotopic substitution is larger.

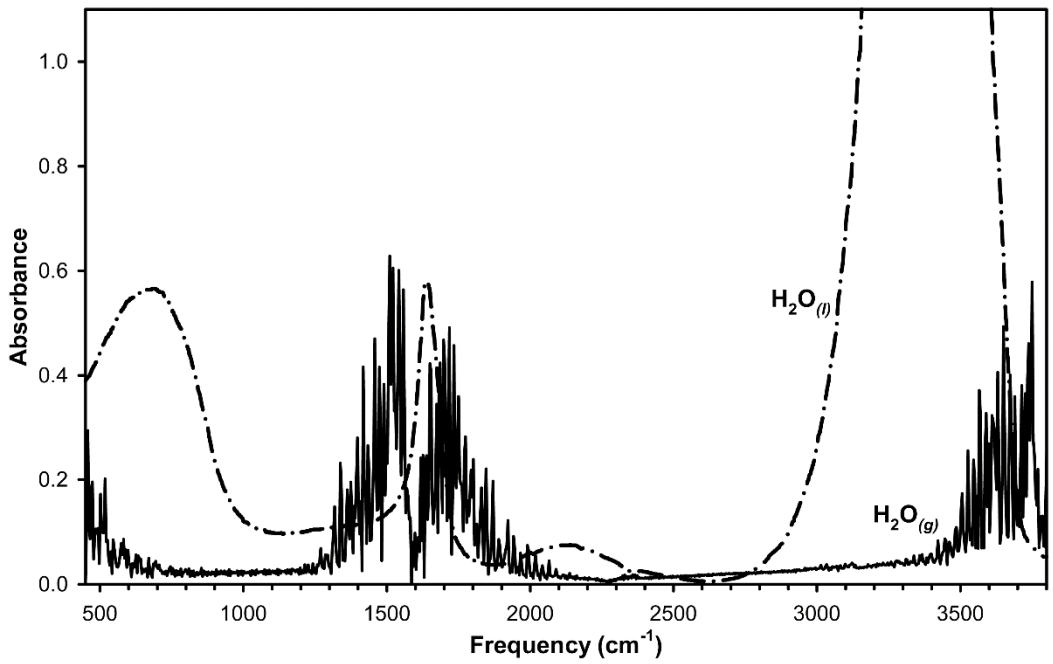

Fig. 1. Broadening of vibrational transitions in condensed phases. Data from NIST Mass Spectrometry Data Center (2020).

These interactions cause narrow, gas-phase vibrational absorption lines to shift and broaden (Fig. 1). Weak long-range interactions, including those arising from long-range order in solids, can comprise an important component of the β^* values in condensed-phase systems. Schauble (2004) introduced the following equation, based on the work of Kieffer (1982), to represent the reduced partition function ratio in terms of a continuum of vibrations in solids:

$$\beta^{¿} = \left(\frac{m}{m^{¿}}\right)^{3/2} \exp\left[\frac{\frac{1}{n}\int_0^{\nu_{max}} \ln\left(\frac{e^{-U^{¿}/2}}{1-e^{-U^{¿}}}\right) g(\nu^{¿})\, d\nu^{¿}}{\int_0^{\nu_{max}} \ln\left(\frac{e^{-U/2}}{1-e^{-U}}\right) g(\nu)\, d\nu}\right] \quad (3)$$

Here, m and m^* are the masses of the normal and rare (commonly heavy) isotope being exchanged, respectively, n is the number of atoms exchanged in a unit cell, and g is the vibrational density of states, which is proportional to the number of vibrational modes in the frequency window between ν and $\nu + d\nu$. The upper frequency limit of the integrals is the highest vibrational frequency ν_{max} in the crystal. Note that the atoms in crystals are neither free to translate nor rotate; thus the translational and rotational terms of the Teller-Redlich isotopic product rule drop out, resulting in the leading $(m/m^*)^{3/2}$ term.

Because many of the terms in eqn. (3) are either uncertain or poorly constrained, one often must approximate it. Elcombe and Pryor (1970) showed that the continuous crystal spectrum of the ionic solid CaF can be well-approximated by using a set of discrete frequencies as constraints on lattice vibrations simulated to satisfy known physical properties (e.g., the

dielectric and elastic constants). This approach has not yet been utilized for predictions of triple oxygen-isotope fractionation, although it has been used to examine bulk $^{18}O/^{16}O$ fractionation factors in minerals (Bottinga 1968; Kieffer 1982; Chacko et al. 1991; Schauble et al. 2006b).

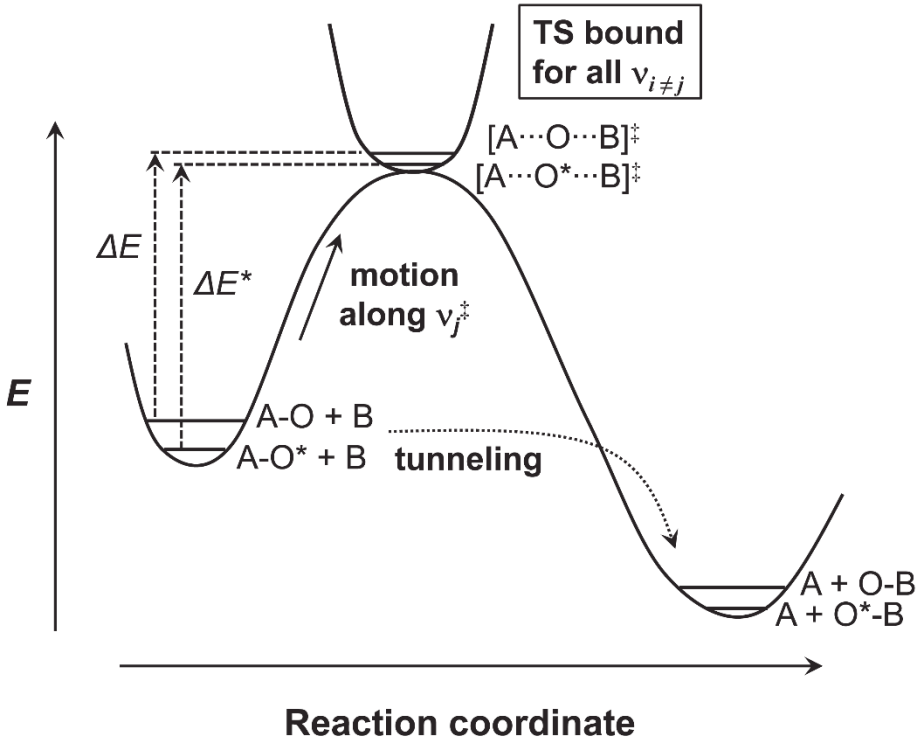

Fig. 2. Schematic of reaction pathway for a generic O-atom exchange reaction.

Kinetic isotope effects are typically approached through the lens of adiabatic transition-state theory (Evans and Polanyi 1935; Eyring 1935) using the schematic depicted in Figure 2. Transition-state theory presumes that reactions proceed first through a pre-equilibrium between the reactants and an activated complex (i.e., a transition state, denoted by a "‡" superscript) followed by a unidirectional transformation of that complex into the products. The transformation of reactant A to product B through a transition state TS would thus be written:

$$A \rightleftharpoons [TS]^‡ \rightarrow B$$

The transition state is saddle point on the potential energy surface, meaning that all nuclear vibrations are bound except that which defines the bond being made or broken. The axis that describes the path of that bond is known as the reaction coordinate (see Fig. 2). The rate of a reaction can be written in terms of the partition functions Q of the reactants (i.e., the product of the partition functions for each reactant) and the transition state:

$$k = \eta_{tun} \frac{k_B T}{h} \frac{Q^‡}{Q_{reactants}} e^{\frac{\Delta E^‡}{k_B T}} \quad (4)$$

Here, η_{tun} is a correction for nuclear tunneling (a uniquely quantum-mechanical effect discussed below) and $\Delta E^{\ddagger}$ is the height of the activation barrier after accounting for zero-point vibrational energy (i.e., $E_{ZPE} = \frac{1}{2} h\nu_0$). The kinetic $^{18}O/^{16}O$ fractionation factor is thus (Bigeleisen 1949; Bigeleisen and Wolfsberg 1958):

$$^{18}\alpha_{kin} = \frac{^{18}k}{^{16}k} = \frac{^{18}\eta_{tun}}{^{16}\eta_{tun}} \frac{^{18}\beta^{\ddagger *}}{^{18}\beta_{reactants}} e^{\frac{\left(\Delta^{18}E^{\ddagger} - \Delta^{16}E^{\ddagger}\right)}{k_B T}} \quad (5)$$

where k is the reaction-rate coefficient and

$$\beta^{\ddagger *} = \frac{\nu_j^{\ddagger *}}{\nu_j^{\ddagger}} \prod_{i \neq j}^{3N-7} \quad (6)$$

The reduced partition function ratio for the transition state, $^{18}\beta^{\ddagger *}$, is nearly identical to that in eqn. (1) except that the vibrational mode j that corresponds to the transforming bond is removed from the ZPE and EXC terms. That mode is unbound because it defines the reaction coordinate (Fig. 2); thus it is not free to vibrate in the transition state. Consequently, it has an imaginary frequency, $\nu_j^{\ddagger}$. The MMI term, however, expressed using the Teller-Redlich product rule, includes this imaginary frequency, so the ratio $\nu_j^{\ddagger *}/\nu_j^{\ddagger}$ remains outside the product. In addition, the η_{tun} terms in eqn. (5) also depend on $\nu_j^{\ddagger}$; they are approximately equal to $1 + U_j^{\ddagger 2}/24$ (Wigner 1932; Bigeleisen and Wolfsberg 1958). Note that these expressions also employ the harmonic-oscillator and rigid-rotor approximations.

Quantifying mass-dependent fractionation

Triple-isotope variations can be quantified in many ways, but we will restrict the present discussion to several recurring terms used in the mass-dependent fractionation literature: κ, θ, and λ (Bao et al. 2016; Dauphas and Schauble 2016). The three terms cover the spectrum of theoretical to empirical quantities, with κ being theoretically straightforward but difficult to verify by experiment, and λ being observationally straightforward but the most difficult to predict directly by theory. Each has its utility for different objectives in oxygen triple-isotope geochemistry.

The triple-isotope κ value is characteristic of isotope-exchange equilibrium between an isotopically substituted species and a free atom. It is defined as the ratio of the natural logarithms of the reduced partition function ratios (Cao and Liu 2011):

$$\kappa = \frac{\ln {}^{17}\beta_A}{\ln {}^{18}\beta_A} \quad (7)$$

This term, while abstract, has the benefit of putting all oxygen triple-isotope variations against a common reference state (atomic oxygen, which has no chemical isotopic preferences). Under the approximations used in eqn. (1), it is bounded in the triple-oxygen system, in the high-temperature limit, to a maximum value of 0.5305 because $\kappa(T \to \infty) = (1/m_{16} - 1/m_{17})/(1/m_{16} - 1/m_{18})$, in which the subscripts denote the isotope masses. Most oxygen-containing species thus far

studied have temperature-dependent κ values lying between 0.527 and 0.530 (Young et al. 2002; Cao and Liu 2011; Hayles et al. 2017; Hayles et al. 2018).

Individual contributions to κ from can be separated by the relation (Hayles et al. 2017):

$$\kappa_{complete} = \frac{\sum_i \kappa_i \ln {}^{18}\beta_i^{\square}}{\sum_i \ln {}^{18}\beta_i^{\square}} \tag{8}$$

in which $\Pi\beta_i = \beta^*$, and β_i (no asterisk) refers to the contributions from individual vibrational modes to β^*. Each pair of ${}^{17}\beta_i$ and ${}^{18}\beta_i$ values thus yields a κ_i value for that mode. The contribution from the imaginary frequency of a transition state in eqn. (6) in this framework is defined as $\beta_{IF}^{\ddagger} = \nu_j^{\ddagger *}/\nu_j^{\ddagger}$. Corrections for deviations from the harmonic-oscillator and rigid-rotor assumptions can also be incorporated this way, allowing one to understand their influence on $\kappa_{complete}$ (see below).

A more empirically tractable quantity is the triple-isotope exponent θ, which describes the triple-isotope fractionation between two species or phases, rather than a single species or phase relative to an atom. The quantity θ is derived from the relation ${}^{17}\alpha_{A\text{-}B} = ({}^{18}\alpha_{A\text{-}B})^{\theta}$ for fractionation factors and is conventionally defined in logarithmic form, i.e.,

$$\theta_{A-B} = \frac{\ln {}^{17}\alpha_{A-B}}{\ln {}^{18}\alpha_{A-B}} \tag{9}$$

Because uncertainties in ${}^{17}\alpha_{A\text{-}B}$ and ${}^{18}\alpha_{A\text{-}B}$ values covary in laboratory measurements, $\theta_{A\text{-}B}$ values for many processes can be derived from laboratory measurements to high precision (Angert et al. 2003; Angert et al. 2004; Helman et al. 2005; Luz and Barkan 2005; Barkan and Luz 2007; Pack and Herwartz 2014b; Sharp et al. 2016; Sengupta and Pack 2018; Stolper et al. 2018; Wostbrock et al. 2018; Ash et al. 2020; Wostbrock et al. 2020); thus, $\theta_{A\text{-}B}$ values have been indispensable as a mediator between experiment and theory. To first order, $\theta_{A\text{-}B}$ values are insensitive of temperature (Young et al. 2002), but experimental and theoretical work has shown that a the subtle temperature dependence can be observed in many cases (Cao and Liu 2011; Pack and Herwartz 2014b; Casado et al. 2016; Sharp et al. 2016; Hayles et al. 2018; Stolper et al. 2018; Wostbrock et al. 2018).

The triple-isotope coefficient λ has multiple meanings in the literature. We will simplify them here as λ and λ_{RL}. The former is descriptive and used to characterize experimentally observed relationships between isotope ratios (e.g., the meteoric water line has $\lambda = 0.528$). In the simplest case, λ describes the differences in δ' values between two species, but more often it describes a best-fit slope for set of measured data, i.e.,

$$\lambda = \frac{\Delta\delta'^{17}_{\square}O}{\Delta\delta'^{18}_{\square}O} \tag{10}$$

The latter quantity λ_{RL}, however, is the reference slope against which Δ'^{17}O values are reported:

$$\Delta'^{17}O = \delta'^{17}O - \lambda_{RL} \times \delta'^{18}O \quad (11)$$

Both of these uses serve empirical ends, and do not necessarily represent discrete processes. However, λ_{RL} is sometimes tied to λ, θ, or κ values for convenience. One prominent example is the high-temperature limit of κ [i.e., 0.5305; (Pack et al. 2013; Pack and Herwartz 2014b)]. We will use $\lambda_{RL} = 0.528$ to report data here unless otherwise specified.

The relationship between observed λ values and the more fundamental θ values relies on an assumed physical model of the system, and thus can vary. For example, for a well-mixed system described by Rayleigh fractionation, one can define $\lambda_{Rayleigh}$ [γ in Angert et al. (2003)] as

$$\lambda_{Rayleigh} = \frac{1 - {}^{18}\alpha^{\theta}}{1 - {}^{18}\alpha} \quad (12)$$

whereas for a diffusion-limited Rayleigh system (He and Bao 2019; Li et al. 2019),

$$\lambda_{diff-rxn} = \frac{1 - \left({}^{18}\alpha\right)^{\theta/2}}{1 - \left({}^{18}\alpha\right)^{1/2}} \quad (13)$$

Using triple-isotope observations to constrain chemical or thermodynamic quantities (e.g., formation temperature) thus requires that one evaluate and understand the physical constraints on a given problem, often through its extended geochemical context.

Note that theory meets the "real world" in these three quantities. The experimentalist will almost always measure α and λ values, which, through suitable model of the system under study, may allow them to infer $\theta_{A\text{-}B}$ values. The theorist will always calculate a set of β^* values first before obtaining α, κ, and $\theta_{A\text{-}B}$ values for fundamental processes. Interpreting subtle variations in triple-oxygen compositions in natural systems thus requires an understanding of how accurate each of these approaches is, or at least how well they are able to reproduce each other.

Natural variability in the triple-oxygen exponents θ

In pursuit of an intuition about triple-oxygen isotope systematics, one may wish to interrogate the bounds of θ values allowed by theory: what are typical ranges for equilibrium and kinetic processes, and when can θ values deviate from these ranges? For equilibrium processes, θ^{eq}_{A-B} can be expressed in terms of κ, ${}^{18}\alpha$, and ${}^{18}\beta^*$ values (Cao and Liu 2011):

$$\theta^{eq}_{A-B} = \kappa_A + \left(\kappa_A - \kappa_B\right) \frac{\ln {}^{18}\beta^{\iota}_B}{\ln {}^{18}\alpha^{\square}_{A-B}} \quad (14)$$

While his expression highlights the larger physically allowable range in θ^{eq}_{A-B} values compared to κ values, which have a maximum value of 0.5305 at high temperatures (see above). When $\kappa_A \neq \kappa_B$, θ^{eq}_{A-B} values diverge for small ${}^{18}O/{}^{16}O$ fractionations, i.e., when $\ln({}^{18}\alpha_{A\text{-}B}) = \ln {}^{18}\beta_A{}^* - \ln {}^{18}\beta_B{}^*$ is

near zero. This divergence allows θ^{eq}_{A-B} to take any value in an isotope-exchange equilibrium in principle; fractionation "crossovers," where $\ln(\alpha_{A\text{-}B})$ changes sign as a function of temperature (e.g., hematite-water equilibrium near 60°C), have been highlighted before as regions where θ^{eq}_{A-B} values can deviate strongly from the limits of κ and yield anomalous isotope effects (Skaron and Wolfsberg 1980; Kotaka et al. 1992; Hayles et al. 2017). Nevertheless, the typically expected range in θ^{eq}_{A-B} values is between 0.525 and 0.530 at Earth-surface temperatures and above, slightly larger than the range for κ values (Bao et al. 2016).

The kinetic triple-isotope exponent θ^{kin}_{A-B} has a typical range that is even larger. Young et al. (2002) first showed, using both transition-state theory and Rice-Ramsperger-Kassel-Marcus theory for unimolecular decomposition (Marcus 1952), that kinetic triple-oxygen isotope effects depend on whether the isotopic substitution is part of the bond being altered. If oxygen-atom motions are only relevant along the reaction coordinate (cf. Fig. 2), then the θ^{kin}_{A-B} value approaches the mass dependence of classical particles in motion, i.e., the relative velocities of ^{16}O, ^{17}O, and ^{18}O, approaching $\theta^{kin}_{A-B} = 0.516$ as the masses of the participant fragments increases or the temperature increases. Within the framework of κ values, eqn. (6) implies that $\kappa_{complete}$ approaches κ_{IF} (the imaginary-frequency contribution to $\kappa_{complete}$) when an isotopic substitution only affects motion along the reaction coordinate (Hayles et al. 2017):

$$\kappa_{IF} = \frac{\ln\left(\frac{{}^{17}\nu_j^{\ddagger}}{{}^{16}\nu_j^{\ddagger}}\right)}{\ln\left(\frac{{}^{18}\nu_j^{\ddagger}}{{}^{16}\nu_j^{\ddagger}}\right)} = \frac{\ln\left(\frac{{}^{17}\mu^{\ddagger}}{{}^{16}\mu^{\ddagger}}\right)}{\ln\left(\frac{{}^{18}\mu^{\ddagger}}{{}^{16}\mu^{\ddagger}}\right)} \tag{15}$$

Here, the reduced mass μ [i.e., derived from $1/\mu = \Sigma\,(1/m)$] corresponds to that of the two fragments participating in the vibration that becomes the reaction coordinate. In contrast, if the oxygen-atom vibrations are all orthogonal to the reaction coordinate, then θ^{kin}_{A-B} approaches θ^{eq}_{A-B}. One might then surmise that if oxygen atoms participate in some vibrational modes of both the reactants and transition state, then θ^{kin}_{A-B} lies somewhere in between the classical limit and θ^{eq}_{A-B} (Dauphas and Schauble 2016). We note that Bao et al. (2015) showed that because θ^{eq}_{A-B} is not bounded—e.g., it adopts unusual values near isotopic crossovers—θ^{kin}_{A-B} can also adopt any value. Nevertheless, this simplified view obscures an important and non-intuitive feature of kinetic fractionation for oxygen triple isotopes: $\theta^{kin}_{A-B}$is not bounded, even for well-behaved reactions far from where the kinetic isotope fractionation changes sign.

The loss of one vibrational degree of freedom in eqn. (6) relative to eqn. (1) is the ultimate origin for θ^{kin}_{A-B} being unbounded. Importantly, the ratio of imaginary frequencies, $\beta_{IF}{}^{\ddagger}$, is always less than one (Bigeleisen and Wolfsberg 1958). If the substituted oxygen atom participates in some vibrational modes of both the reactants and products, then the remaining, real portion of $\beta^{*\ddagger}$ in eqn. (6) is greater than one (i.e., $\beta_{real}{}^{\ddagger} > 1$). This disparity in β_i values on either side of unity creates an "internal crossover" for $\kappa^{\ddagger}$: the denominator of eqn. (8) for the transition state, $\ln{}^{18}\beta_{IF}{}^{\ddagger} + \ln{}^{18}\beta_{real}{}^{\ddagger}$, is predisposed to be close to zero. $\kappa^{\ddagger}$ itself is not bounded, and instead is predisposed to appear anomalous. Higher values of ${}^{18}\beta_{real}{}^{\ddagger}$, arising from lower reaction

temperatures and/or substitutions that shift high-frequency vibrations, tend to drive $\kappa^{\ddagger}$ toward a canonically more "normal" range. To illustrate this concept, we plot predicted values of $\kappa^{\ddagger}$ for a variety of model transition states as a function of ${}^{18}\beta^{\ddagger *} = {}^{18}\beta_{IF}{}^{\ddagger} \times {}^{18}\beta_{real}{}^{\ddagger}$ in Figure 3. A $\kappa^{\ddagger}$ crossover can be seen at ${}^{18}\beta^{\ddagger *} = 1$ (i.e., $\ln{}^{18}\beta_{IF}{}^{\ddagger} + \ln{}^{18}\beta_{real}{}^{\ddagger} \sim 0$), with anomalous nearby $\kappa^{\ddagger}$ values. Given this predisposition for high variability in $\kappa^{\ddagger}$, then, the values of θ^{kin}_{A-B} typically measured and calculated, between 0.516 – 0.53 (Bao et al. 2016), are surprising. The absence of anomalous θ^{kin}_{A-B} values in the literature imply that bounds on its value are imposed by chemical and not mathematical limits.

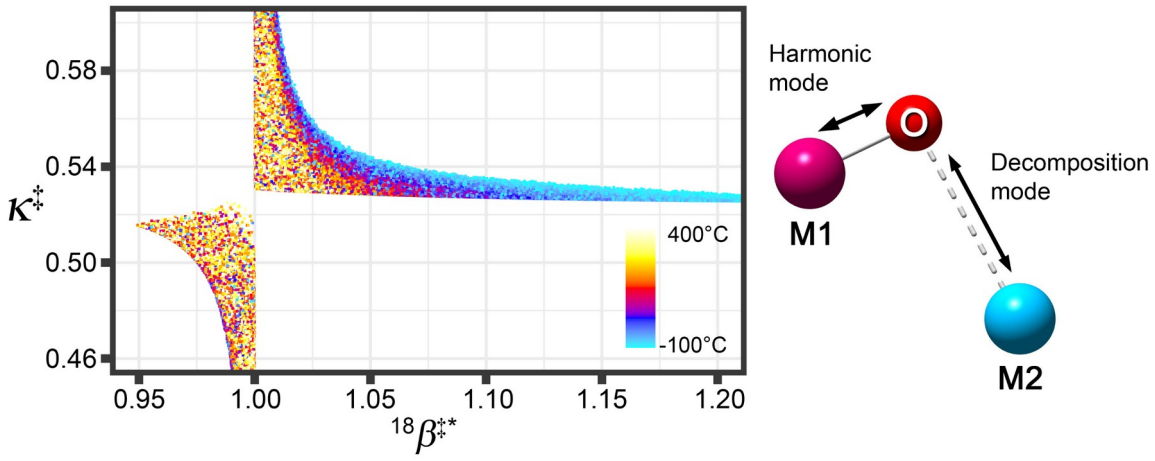

Fig. 3. Monte-Carlo sampling of ${}^{18}\beta^{\ddagger *} = {}^{18}\beta_{IF}{}^{\ddagger} \times {}^{18}\beta_{real}{}^{\ddagger}$ and $\kappa^{\ddagger}$ values for a model transition state. In this model, the harmonic vibration of a diatomic molecule M1—O is used to obtain ${}^{18}\beta_{real}{}^{\ddagger}$, the real portion of eqn. (6). The force constant for that bond is varied from that of CO to 1/8th that of CO. The imaginary frequency contribution to eqn. (6), ${}^{18}\beta_{IF}{}^{\ddagger}$, is here equal to $(\mu_{M1—O+M2}/\mu_{M1—O^*+M2})^{1/2}$, i.e., a function of the reduced mass along the decomposition mode only. Both M1 and M2 are varied from 1 – 300 amu for Monte Carlo sampling. For comparison, the harmonic vibration of O_2 (ν = 1580 cm^{-1}) ${}^{18}\beta_{real}{}^{\ddagger} = 1.17$ at 25°C.

Nuclear tunneling is thought to be negligible for oxygen atoms, leading to the generalizations above [cf. eqns. (4) and (5)]. However, electron-nuclear tunneling may be relevant in electron-transfer (ET) reactions, which are ubiquitous in biology (Bertini et al. 1994). In this mechanism, electron tunneling through the reaction barrier results in nuclear reorganization, especially at low temperatures (De Vault and Chance 1966; Hopfield 1974); the nuclear motions in this case are a response to the reaction, not the cause of it (*sensu stricto*). Its mass dependence is not obvious at first glance.

Two mechanisms of ET reaction are relevant: Inner-sphere and outer-sphere. Inner-sphere electron transfer involves bond-making and/or breaking, whereas outer-sphere electron transfer does not. The former mechanism is characteristic of enzyme catalysis and has oxygen-isotope effects arising from both transition-state properties and tunneling (Roth et al. 2004; Mukherjee et al. 2008). The latter type describes all long-range electron transfers in biological systems (Bertini et al. 1994) and has isotope effects arising primarily from electron-nuclear tunneling. We explore the mass dependence of the latter mechanism below.

Buhks, Jortner, and coworkers (Buhks et al. 1981a; Buhks et al. 1981b) described outer-sphere electron transfer in terms of an electronic coupling term (i.e., the probability of an ET event) and a Franck-Condon overlap factor (i.e., for a given geometry in a given system). The latter term encompasses the Franck-Condon principle, which states that an electronic transition is most likely to occur between states that resemble each other on the potential energy surface. For example, the half-reaction $O_2 + e^- \rightarrow O_2^-$ is most likely to occur when the O-O bond length in O_2 (1.21Å on average) is equal to the equilibrium bond length of O_2^- (1.28Å). Note that changes in the O-O bond length occur naturally as the O_2 molecule vibrates, modulating this overlap (Fig. 4, left). The equations describing the tunneling effects on the reaction $O_2^* + O_2^- \rightarrow O_2^{-*} + O_2$ are:

$$Y = \frac{4\pi(\Delta d)^2 \nu_r \nu_p}{\nu_r \coth\left(\frac{U_p}{4}\right) + \nu_p \coth\left(\frac{U_r}{4}\right)} \tag{16}$$

$$(\Delta d)^2 = \frac{2\pi\mu(\Delta r)^2}{h} \tag{17}$$

$$\ln\alpha = Y - Y^{\dagger} \tag{18}$$

Here, $(\Delta r)^2$ is the squared change in equilibrium bond length between reactant (subscript r) and product (subscript p). For harmonic oscillators, the $(\Delta r)^2$ term and the constants cancel when θ values are computed, rendering the difference between ν_r and ν_p (i.e., the change in bond strength upon reaction) the most important factor that determines θ^{ET} for the ET component of these reactions.

We compared the ET and equilibrium θ values for the reaction $O_2^* + O_2^- \rightarrow O_2^{-*} + O_2$ using known harmonic vibrational frequencies of 1580 cm^{-1} and 1090 cm^{-1} for the neutral and anionic $^{16}O^{16}O$ species, respectively (Celotta et al. 1972; Huber and Herzberg 1979). The results between 0°C and 400°C are shown in Figure 4. Interestingly, the outer-sphere electron transfer mechanism is not mass-anomalous, as one might have guessed for an electron tunneling-driven reaction, or from the dependence of α on $(\Delta r)^2$. Instead, θ^{ET} is well behaved and less than θ^{eq} over the entire temperature range. Therefore, a kinetically limiting outer-sphere ET pathway has a mass dependence in the range of more typical kinetic isotope effects: the range in θ^{ET} values is still between 0.52 and 0.53 in this temperature range.

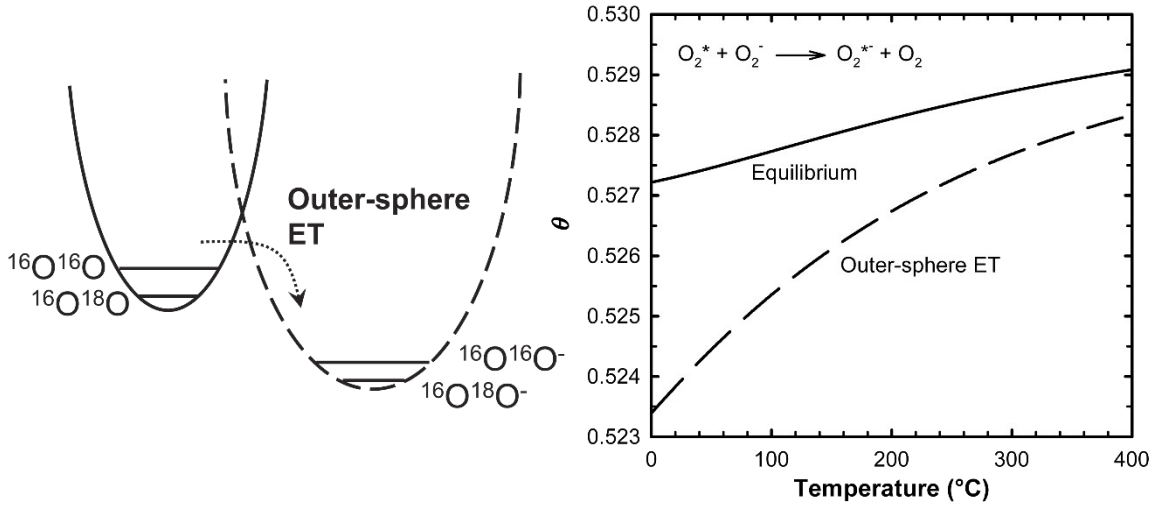

Fig. 4. Effects of outer-sphere electron transfer in the reaction $O_2^* + O_2^- \rightarrow O_2^{-*} + O_2$. (Left) Schematic depicting outer-sphere ET through electron-nuclear tunneling. (Right) Comparison of θ values between 0°C and 400°C predicted for outer-sphere ET and isotopic equilibrium.

The preceding discussion emphasizes the relatively small range of triple-isotope fractionation exponents observed, and the broader range allowed by theory in geochemical systems. These ranges set a target on how accurate theoretical predictions and measurements need to be in order to interpret isotopic trends unequivocally. Systems showing higher variability in θ values such as those influenced by isotopic crossovers, photochemistry, surfaces, and/or low temperatures (Skaron and Wolfsberg 1980; Horita and Wesolowski 1994; Abe 2008; Balan et al. 2009; Sun and Bao 2011; Eiler et al. 2013; Hayles et al. 2017) may have slightly lower accuracy requirements, but their influence in nature is no less important to understand.

A note about anharmonicity

The assumptions present in eqs. (1), (3), (6), and (15) are nontrivial, so an exploration of their effects on calculated triple-isotope fractionation is warranted. The harmonic-oscillator and rigid-rotor approximations, in particular, represent idealized behaviors of atoms and bonds, and are generally justified if molecules primarily occupy the lowest vibrational state (e.g., under mild conditions). Relaxing the harmonic oscillator and rigid-rotor assumptions allows vibrational and rotational modes to influence each other and centrifugal forces to affect bond lengths. More subtle molecular motions, such as hindered internal rotations, may also be relevant. Collectively, these are known as anharmonic effects. While accounting for these effects adds considerable complexity to calculations, it also yields a more accurate description of the physical system and more accurate isotopic fractionations in principle.

Richet et al. (1977) and Liu et al. (2010) found that the most significant anharmonic effect for isotopic fractionation is that associated with the lowest vibrational state. While this anharmonic correction can be calculated from spectroscopic constants for some simple molecules, a more typical treatment is to replace the *ZPE* term in in eqn. (1) with an anharmonic

zero-point energy obtained directly from electronic structure programs. The resulting expression for β^*, incorporating this first-order correction, is thus:

$$\beta'_{anharm} = \left(\frac{e^{-ZPE'_{anh}/kT}}{e^{-ZPE_{anh}/kT}} \right) \prod_i \left(\frac{\nu'_i}{\nu_i} \right)_{MMI} \left(\frac{1-e^{-U_i}}{1-e^{-U'_i}} \right)_{EXC} \quad (19)$$

where ZPE_{anh} is the total anharmonic vibrational zero-point energy of the molecule. These effects are most pronounced for molecules bearing light elements such as hydrogen.

While the accuracy benefits of anharmonic corrections are apparent for individual β^* and α values, there is a certain degree of error cancellation for mass-dependent processes. The accuracy improvements for the quantities κ and θ in the oxygen triple-isotope system therefore are not as obvious. Calculating anharmonic effects is expensive, and may be of limited use if the end result is nearly unchanged from the harmonic result. Cao and Liu (2011) found that The anharmonic correction typically accounts for single-digit percentages of $\ln(^{18}\beta^*)$ for hydrogen-bearing molecules and even less for non-hydrogen bearing species. For small molecules (i.e., CO_2 and N_2O), changes to κ values arising from anharmonic effects were therefore found to be <0.0001. The negligible importance of anharmonic effects for κ values has not yet been evaluated for oxygen-isotope exchange reactions in condensed phases, so it may be premature to rule out completely. We will proceed acknowledging this uncertainty.

ELECTRONIC STRUCTURE CALCULATIONS

The central consideration for applying theoretical chemistry to triple-isotope fractionation is the electronic structure calculation. Accurate vibrational frequencies rely on an accurate calculation of the potential energy experienced by the nuclei—i.e., the potential energy surface, so more accurate electronic structure predictions should lead to more accurate triple-isotope fractionation predictions. However, myriad factors influence the accuracy of the predictions: First, what is the molecular model being investigated, and how well does it represent the real system of interest? Second, how are the chemical (i.e., electronic) interactions being treated by the chosen electronic structure method? Third, how are electrons being represented in the calculation, i.e., what set of basis functions is being used to describe their distribution? A discussion of these factors, and their potential importance for first-principles isotopic fractionation calculations, follows below.

Molecular models

In systems containing only a few atoms, such as gas-phase atmospheric reactions, the molecular model often closely approximates the real system; thus the limitations on accuracy in the gas phase generally revolves around the electronic structure method and basis functions used. Key details about the electronic configuration, e.g., electron spins in open-shell molecules, become the most important elements in the model to consider. In contrast, long-range interactions in condensed phases that must be tackled using finite computing resources forces the investigator to truncate solid and liquid systems in a meaningful way. The optimal molecular

model in that case is an approximation of the geochemical system that recovers sufficient accuracy to be useful (Schauble 2004). Two basic approaches to approximation have emerged: cluster models and lattice-dynamics models.

Cluster models simulate only a small portion of a crystal or liquid. They can be accurate if isotopic substitutions are rare and only affect vibrational frequencies local to the substitution. Long-range interactions (e.g., acoustic lattice vibrations) are omitted in order to simulate the vibrational modes near the isotopic substitution more accurately. Rustad and Liu, among others, have utilized these models extensively for isotopic equilibrium calculations in solvated and crystalline species (Rustad et al. 2008; Rustad et al. 2010; Li and Liu 2015; Hayles et al. 2018). Each cluster contains the local crystal (or liquid) structure around a subunit that contains several "shells" of atoms around the target chemical species (e.g., bonds around a central SiO_4 tetrahedron in quartz). For mineral models, the edge of the cluster is truncated in some way, either by replacing the broken bonds with hydrogen to generate a neutral cluster (where appropriate), or by embedding an ionic cluster within an appropriate array of point charges. The minimum number of shells/bonds around the isotopic substitution is generally taken to be three—one fixed outer shell and at least two inside that are free to vibrate (Rustad et al. 2008; Rustad et al. 2010)—with larger clusters and more vibrating shells yielding higher accuracy and diminishing returns for more computational time (i.e., scaling roughly with the number of electrons raised to the 3rd or 4th power). Vibrational frequencies are calculated using electronic structure methods [e.g., commercial software packages Gaussian, Q-Chem, and Turbomole, and open-source or freeware software GAMESS, NWChem, and Quantum Espresso (Schmidt et al. 1993; Valiev et al. 2010; Furche et al. 2014; Shao et al. 2015; Frisch et al. 2016; Giannozzi et al. 2017)]. The discrete results are inputted into the Bigeleisen-Geoppert-Mayer-Urey formula [eqn. (1)] to obtain isotopic fractionation factors.

An alternative approach to cluster models is to simulate a more extended crystal structure, and thus the long-range interactions, using a lattice-dynamics approach (Elcombe and Hulston 1975; Dove et al. 1992; Schauble et al. 2006a; Yeung et al. 2012; Blanchard et al. 2017). A larger number of atoms is simulated, often with periodic boundary conditions, to recover the broad spectrum of lattice vibrations relevant to the phase. To mitigate the added computational burden of simulating more atoms, the electronic structure calculation is simplified further by assuming that only valence electrons of each atom interact with each other. The electrons in core atomic orbitals are replaced with a pseudopotential, a stand-in for the electronic potential energy of the atomic core; many open-source databases are available online. Shortcomings of this method include its semi-empirical nature, and to our knowledge this approach has not been used for triple-oxygen isotope predictions. Lattice dynamics-based isotopic fractionation predictions for the carbonate clumped-isotope system are lower than those computed using the cluster method (Schauble et al. 2006a; Zhang et al. 2020).

Ultimately, a theoretical calculation can only be as accurate as its molecular model. Ways of verifying the accuracy of a model include comparing its harmonic vibrational frequencies against experimental harmonic frequencies; however, only observed spectroscopic frequencies (which include anharmonicity) are typically available for condensed phases. The electronic structure calculation method often introduces additional bias, so uncertainties remain in many cases (see below). Hayles et al. (2018) used two clusters of different sizes to test the convergence

of their results, an approach that we recommend as a practical test of systematic errors. However, the omission of long-range lattice modes in all cluster models could still result in errors.

Electronic structure methods: different ways of treating chemical interactions

Electronic structure calculations generally fall under two approaches. The first is wavefunction theory, which aims to describe a molecule by its electronic wavefunction; that wavefunction is used in the Schrödinger wave equation to obtain molecular properties. The most elementary computational approach to obtaining molecular wavefunctions is the Hartree-Fock (HF) method, which assumes that electrons only interact with positively-charged nuclei and an mean field of negative charge arising from other electrons (Jensen 2017). Pairwise and many-body electron-electron interactions (electron correlation) are omitted in that energy calculation. Moreover, relativistic effects relevant to transition metals are ignored. Clearly, these assumptions comprise a severe approximation of the real behavior of electrons, resulting in low accuracy in all but the simplest, closed-shell systems. Treatment of electron correlation is possible, often by either perturbing the mean-field approximation using a correlation potential (e.g., second-order Møller-Plesset perturbation; MP2) or by allowing electronic configurations other than the ground state to influence the ground-state energy (e.g., configuration interaction/CI or coupled cluster/CC approaches). Increasing the number of configuration interactions gives a predictable march toward increased accuracy—an important consideration if molecular structures cannot be linked to observables (e.g., transition states). However, these corrections are computationally expensive, especially in larger systems, because each electron and configuration must be individually considered and computed; continued advances in implementation are reducing the cost of these calculations (Peng et al. 2016; Vogiatzis et al. 2017). At present they are not widely used in isotopic calculations, although they may be affordable for small gas-phase systems.

The second and most-often used electronic structure method in geochemistry is density functional theory (DFT). It conceptualizes the electronic configuration as the electron density in three dimensions in space (i.e., number of electrons per unit volume) rather than a collection of constituent electronic wavefunctions (Becke 2014; Peverati and Truhlar 2014). Therefore, instead of solving the many-body interaction problem directly as HF approaches do, modern DFT methods—Kohn-Sham DFT being the most common—break up the electronic energy into separable components comprised of (1) coulombic electron-nuclei interactions, (2) electron kinetic energy in the absence of electron-electron interactions, (3) coulombic electron-electron repulsion, and (4) energy associated with electron exchange and correlation[1]. Each is a function of the total electron density, and can be computed separately, increasing efficiency. The electron density is varied until energy is minimized. In principle, this approach can recover the molecular wavefunction exactly, provided the function describing the electron density is known. In practice, however, one can only approximate the true electron density, resulting in an approximate description of the electronic energy (which is a *functional* of the electron density).

The first three components of the Kohn-Sham DFT method are straightforward to compute, but the last component is wrought with particular difficulty. One can choose functional forms and the associated parameters for exchange and correlation that are based in physical

[1] Electron exchange energy is the tendency for two electrons of the same spin to avoid each other. The effective repulsion arises from the Pauli exclusion principle of quantum mechanics. Electron correlation energy is associated non-coulombic electron-electron interactions arising from the wave nature of electrons.

constraints, but some functionals often require empirical tuning to maximize accuracy through the use of a benchmark molecular training set that has limited relevance to geochemistry. Other functionals construct a hybrid between HF and DFT methods (with relevant contributions of each optimized similarly) to exploit the advantages of each approach. Developments in DFT focus on improving various representations of exchange and correlation, which have yielded good accuracy in the structure and thermodynamics of an increasingly broad range of materials; however, not all approaches are appropriate for all systems, and unlike wavefunction methods, the path to increased accuracy is not always clear (Mardirossian and Head-Gordon 2017). The "alphabet soup" of DFT methods unfortunately yields little insight. Below we will explore what these developments portend for the isotope geochemist, as well as investigate their consequences for oxygen triple-isotope fractionation predictions specifically. The reader is directed to Becke (2014) and Peverati and Truhlar (2014) for more detailed reviews on DFT.

DFT methods generally differ the most by how they treat the exchange-correlation term, and an appropriate starting point for its discussion is the local spin density approximation (LSDA). In the LSDA, the electron exchange and correlation energy at a given point in space is assumed to be a function of the local electron density only, with the energy equal to that of a "gas" of uniformly distributed electrons at that density. This first approximation yields good molecular geometries, but poor bond- and reaction-barrier energies (Peverati and Truhlar 2014). One can make a higher-order correction to the LSDA (akin to a Taylor expansion about the LSDA minimum) that considers also the local change in electron density. This family of approaches is thus known as the generalized gradient approximation (GGA) family of methods. Further improvements can also be made, such as a consideration of not only the first derivative (gradient) of the electron density, but also its second derivative (i.e., its curvature). This approach is known as a meta-GGA approach. Finally, HF and DFT can be hybridized owing to the equivalency of their descriptions of electronic structure. Hybrid methods incorporate the exchange energy calculated from the HF method to improve the DFT exchange-correlation energy. The exact amount of HF exchange energy used in a hybrid method is most often optimized against chemical properties in a benchmark molecular database. Additional parameters used to improve the performance of long-range interactions have also been employed, and include the development of range-separated and double-hybrid functionals, which have shown great promise (Grimme 2006; Su et al. 2018). The most popular DFT method in the chemical sciences is B3LYP, a semiempirical hybrid GGA functional utilizing three fit parameters that result in 20% HF exchange (Lee et al. 1988; Becke 1993). In contrast, the PBE and TPSS (and later RevTPSS) functionals are pure GGA and meta-GGA functionals with no empirically fit parameters; rather, their forms arise from more detailed treatments of the physical behavior of electrons. Broadly, these incremental improvements to DFT have been likened to rungs on Jacob's ladder (Perdew and Schmidt 2001), with thermodynamic accuracy improving as LSDA → GGA → meta-GGA. Hybrid approaches perform exceedingly well for their training sets, and even beyond them as well; they are often placed above meta-GGAs in the ladder, although they may sometimes perform poorly for cryptic reasons (Paier et al. 2007). In general, the performance of DFT methods for a variety of problems, in isotope geochemistry and beyond, is quite remarkable, despite some consternation in the theoretical chemistry community over the use of semiempiricism (Medvedev et al. 2017).

It is worth noting that treating electron-electron repulsion in terms of electron density has a fundamental problem: an electron cannot repel itself. Yet, the density functional describing

electron-electron repulsion would predict otherwise. In principle, proper calculation of the electron correlation energy will cancel this interaction, but the exchange-correlation functional is only approximate in practice. This problem is thus only partially accounted for in the approximate treatment of electron exchange and correlation, and despite schemes to correct for it (Perdew and Zunger 1981), the "electron self-interaction problem" in DFT remains a sticking point for many theorists.

For the isotope geochemist, the choice of electronic structure method will affect the accuracy of the vibrational frequencies obtained, and thus also the accuracy of isotopic fractionation calculations. Indeed, agreement between theory and experiments for molecular geometries and energies tends to improve as one moves up Jacob's ladder, but the results for vibrational frequencies are not as clear for geologic materials. Comparison of DFT-derived harmonic frequencies with those obtained through high-level wavefunction theory for a suite of molecules reveals biases that vary in both magnitude and sign, with some dependence on the orbital basis set used (Kesharwani et al. 2015; Kashinski et al. 2017). This non-systematic variability may be an artifact of how density functionals are obtained and optimized, and results in a wide range of empirical scaling factors. In practice, direct comparisons of DFT and high-level wavefunction calculations for portions of the system being studied [e.g., (Guo et al. 2009)] may lend additional confidence in the veracity of the results; however, these calculations may not always be available or affordable. Comparing isotopic fractionations calculated at the same theory and basis set is another approach that could mitigate the poorly characterized systematic errors in DFT methods, but its effectiveness has not been thoroughly evaluated.

Representing electrons using basis sets

The third element to an electronic structure calculation is the set of building blocks used to construct the electron density distribution of a molecule. These building blocks are known as basis functions for atomic orbitals, prescribed collections of which are known as basis sets. These electron distributions around atoms are combined in linear combinations to form molecular orbitals. The primitive functions most often utilize Gaussian functions to describe the radial electron density distribution (a reasonable approximation that also facilitates efficiency in computation) plus a separable spherical-harmonic component to describe the shape of the atomic orbital (e.g., *s*, *p*, *d*, and *f* atomic orbitals). For efficiency, core orbitals are often described with fewer terms or *contracted*. Additional Gaussian functions are used to increase flexibility in the radial distribution because electron densities can decrease with nuclear distance in a variety of ways. Using two functions to describe this long-distance falloff yields a "double-zeta" basis function, while using three functions yields a "triple-zeta" basis function, and so forth. In addition, mixed atomic orbital character can be introduced (e.g., *s*-orbitals can take on a little *p*-character when chemical bonds are made), resulting in *polarization* functions that further improve optimized electronic structures. Finally, one can add diffuse functions that focus on capturing the electron density at very large distances from the nucleus. Those are most useful for anionic and other large molecular systems with partial charges. The reader is directed to the review by Jensen (2013) for further details about how they are developed.

Basis sets are named descriptively, although each family tends to have its own scheme. For example, the 6-31G* basis set [equivalent to 6-31G(d)] represents each core orbital shell using a linear combination of six gaussian functions, while each valence orbital is represented

with three and one gaussian functions to describe the inner and outer regions of the valence shell, respectively (Hehre et al. 1972; Hariharan and Pople 1973). Splitting orbitals into inner and outer regions makes it a double-zeta basis set, while treating core and valence electrons differently makes it a split-valence basis set. The addition of the asterisk or "(d)" means that *p*-orbitals can polarize to incorporate *d*-orbital qualities.

Using a high-zeta basis set that includes at least some of the basis function extensions listed above should lead to convergence to the "true" electron density and accurate chemical and isotopic predictions. However, even a moderately-sized chemical system can quickly render a large basis set impractical to use, especially when one might also be able to pair a higher level of electronic structure theory with the smaller basis set. The rate of convergence to the full-basis-set limit becomes key, and depends somewhat on how each basis set is derived. These factors largely govern the choice of basis set in an electronic-structure calculation.

For example, the widely used "Pople" basis set family (e.g., 6-31G) were initially constructed in the 1970s and 1980s from atomic orbitals obtained through HF calculations (Ditchfield et al. 1971), with the addition of MP2 calculations for the triple-zeta basis set 6-311G. While Pople basis sets show good performance for a variety of molecules, the omission of electron-electron correlation in HF calculations causes errors that can propagate to molecular geometries, particularly in delocalized systems (Moran et al. 2006). The "Dunning" or correlation-consistent basis sets (e.g., cc-pVDZ, where "pV" indicates polarized valence and "DZ" indicates double-zeta) first introduced in the 1980s and 1990s were a significant step up: using polarized valence orbitals derived from CI-based atomic calculations, they tend to yield more accurate results than Pople basis sets (Dunning 1989). They are so accurate that decades later, high-zeta Dunning basis sets are still considered the pinnacle of accuracy in wavefunction theory calculations. However, they are costly, converge slowly, and were not optimized for DFT calculations. Subsequent improvements have yielded many other basis set families, notably among which are the "Karlsruhe" basis sets [e.g., def2-SVP, a double-zeta basis set where "SVP" stands for split-valence polarized; (Weigend and Ahlrichs 2005)]. The Karlsruhe basis sets are similar to the Dunning basis sets, but are much more efficient and suitable for a larger portion of the periodic table. A recent DFT basis-set intercomparison showed that, at least for weakly bound complexes, the Karlsruhe basis sets converged toward the complete-basis-set limit faster than Dunning basis sets, with similar performance sometimes achieved with roughly half the number of basis functions (Witte et al. 2016).

We note that basis sets are not restricted to Gaussian-type orbitals. "Slater-type" orbitals, which are more strongly peaked near the nucleus and slower to decay at a distance, were historically the first ones introduced to describe atomic orbitals. However, they were not as computationally efficient or flexible as the Gaussian-based description. Also, lattice-dynamics models use plane-wave basis functions in conjunction with core psuedopotentials (Kresse and Furthmüller 1996; Schwerdtfeger 2011).

Finally, we will mention the basis set superposition error (BSSE), an artifact of incomplete basis sets that may be relevant for the calculation of transition states and aqueous-phase clusters. The error arises from the tendency for each component of a weakly bound complex to utilize the basis functions of the other component(s), erroneously increasing the size of the basis set. The BSSE manifests as an artifactual stabilization of bonds in weakly bound

complexes and thus bond lengths that are too short, as well as vibrational frequency shifts that are too large upon binding (Hermida-Ramón et al. 2003; Hermida-Ramón and Graña 2007). Moreover, while BSSE errors are well known for minimum-energy structures, they are also important for transition states (Kobko and Dannenberg 2001). The counterpoise correction for BSSE, available in many electronic-structure programs, often yields a sufficient first-order correction for the error (Boys and Bernardi 1970). It involves calculating the energies of both the complex and the isolated monomers of the complex in their complexed geometry using the complete basis set of the complex (i.e., each monomer with a "ghost" partner). The BSSE is a potential hazard to the isotope geochemist using affordable basis sets to simulate complex molecular clusters and transition states, although to our knowledge the effect of BSSE on calculated isotopic fractionation has not been investigated.

A preliminary investigation of basis set effects on isotopic fractionation on bioinorganic oxyheme complexes suggests that discrepancies within a family (e.g., Pople, Dunning, or Karlsruhe) are small, but not negligible [i.e., ~1‰ in $^{18}O/^{16}O$ fractionation and ~0.001 in θ^{eq} value; (Ash et al. 2020)]. However, we are not aware of any systematic investigations of basis-set accuracy for high-precision isotope measurements. Large systems, in particular, may not be approachable with expensive triple-zeta basis sets or diffuse functions; if smaller basis sets can suffice by capturing the vibrational frequencies well enough, then many more computationally tractable systems may exist than commonly thought.

Key takeaways

Each of the three components mentioned above—the molecular model, electronic structure method, and basis set—could have varied consequences for high-precision geochemical calculations. While isotope geochemists are typically not as concerned with bulk thermodynamic quantities (e.g., atomization or ionization energies), the practitioner should be familiar with the potential strengths and weaknesses of the available tools: A calculation can only be as good as the molecular model of the real system; newer or more sophisticated DFT methods may not necessarily be more accurate because of potential over-fitting to unrelated test molecules; basis-set size, form, and convergence rate all matter for high-precision accuracy. We believe that the elusive intersection of theory, experiment, and reality at the top of Mount Fuji will appear not by chance, but through the careful selection of methods and evaluation of potential biases in all approaches.

A COMPARISON OF THEORETICAL METHODS

How do the preceding methods affect isotopic fractionation calculations, and oxygen triple-isotope calculations in particular? One might imagine that nearly all of the aforementioned complications will affect the usefulness of calculated triple-oxygen fractionation factors if the target accuracy is at the ppm level in $\Delta'^{17}O$ values. However, do error cancellations in the calculation of triple-isotope trends render these methodological imperfections moot? It is clear from the literature that fortuitous error cancellation occurs for θ values in certain systems [e.g., O_2-heme binding (Ash et al. 2020)]. The harmonic-oscillator approximation used to estimate

vibrational frequencies upon isotopic substitutions renders subtle (<10%) absolute frequency errors less important for θ values if the relative errors are shared for both ^{17}O and ^{18}O substitutions. Yet, the same cannot be said for bulk $^{18}O/^{16}O$ fractionation factors, which are often used as an independent constraint on geochemical problems when paired with θ values (Pack and Herwartz 2014a; Young et al. 2014; Sharp et al. 2016; Hayles et al. 2019).

Approach

We investigated the methodological dependence for the triple-isotope fractionation between crystalline quartz and SiO_2 gas (which is chemically similar to quartz, stable, and easily modeled). The molecular model for crystalline quartz is a cluster model similar to that of Rustad et al. (2008) and Hayles et al. (2018) in which all atoms within five bonds of the central Si, as well as some bridging Si atoms, are included to make a cluster with a stoichiometry $Si_{23}O_{52}^{12-}$. Starting bond lengths and geometries are taken from the American Mineralogist Crystal Structure Database (Levien et al. 1980; Downs and Hall-Wallace 2003). Dangling bonds at the edges, which in this case all have a Pauling bond strength of 1, are replaced with hydrogens, making a final, neutral cluster with the stoichiometry $H_{36}Si_{23}O_{52}$ (Fig. 5). Calculations proceed as follows: First, the hydrogen bond lengths are optimized at the specified level of theory and basis set with all other atoms fixed in their experimentally determined positions. Next, the internal atoms within four bonds from the center are geometry optimized with the remaining atoms fixed in place. Finally, harmonic vibrational frequencies are obtained from the optimized, partially fixed structure. Optimized structures and harmonic vibrational frequencies for SiO_2 gas were calculated using the same theoretical method. Quartz-$SiO_{2(g)}$ isotope fractionations were calculated using eqs. (1), (7) and (14). Adherence to the Teller-Redlich product rule for the quartz models [i.e. *MMI* term of $(m/m^*)^{3/2}$ due to a lack of vibrations and rotations] was within 3 ppm in all cases.

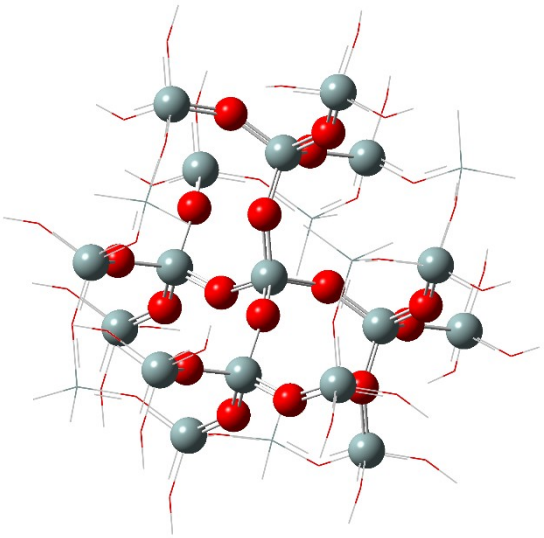

Fig. 5. Embedded quartz cluster used in the electronic-structure method intercomparison. "Frozen" atoms are shown as lines, with the colors distinguishing the different atoms (gray: Si, red: O, white: H).

A total of eight DFT levels of theory were studied, spanning four rungs of "Jacob's ladder": pure GGA (BLYP, PBE), meta-GGA (M11-L, RevTPSS), hybrid GGA (B3LYP, PBE0), and hybrid meta-GGA (M11, TPSSh) (Perdew et al. 1996; Adamo and Barone 1999; Staroverov et al. 2003; Tao et al. 2003; Perdew et al. 2009; Peverati and Truhlar 2011; 2012). We note that the M11 and M11-L functionals are optimized to reproduce observable physical quantities for a large suite of molecules, whereas the others are optimized to reproduce the physical behavior of electrons. Triple-zeta basis sets were not affordable for this intercomparison, so the double-zeta orbital basis sets 6-31G(d), cc-pVDZ, and def2-SVP were used to investigate differences between basis set types. In total, 24 unique electronic structure calculations were performed. Then, we compared the results to a published benchmark B3LYP calculation for a larger quartz cluster model calculated using the triple-zeta 6-311G(d) basis set. That quartz cluster was part of a set of calculations that yielded good agreement with experimental triple oxygen-isotope fractionations between quartz and liquid water (Sharp et al. 2016; Hayles et al. 2018; Wostbrock et al. 2018). We performed new calculations on SiO_2 at the same level of theory and basis set for this comparison. Figure 6 shows the isotopic trends derived from these benchmark calculations compared with available observations, which are generally within 3‰ and 0.001 in $^{18}O/^{16}O$ fractionation and θ^{eq} value at 25°C and below for quartz in equilibrium with liquid water.

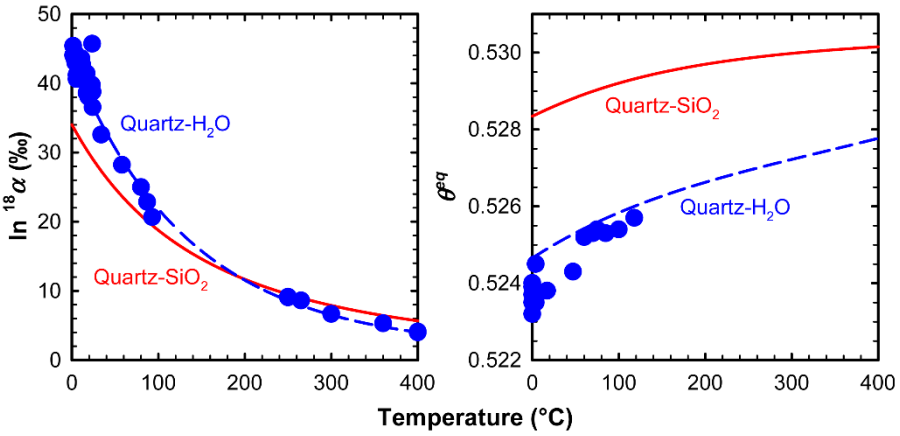

Fig. 6. Theoretical quartz-$SiO_{2(g)}$ and quartz-$H_2O_{(l)}$ fractionation trends, derived from B3LYP/6-311G(d) calculations on a larger embedded quartz cluster used as a benchmark for the methodological intercomparison (Hayles et al. 2018). Blue points are a compilation of empirically determined quartz-$H_2O_{(l)}$ fractionation factors [Sharp et al. (2016), Wostbrock et al. (2018), and references therein].

Results

Table 1 compares the average Si-O bond lengths obtained for the central silicate tetrahedron in the optimized embedded quartz clusters to that measured by high-resolution X-ray diffraction (Levien et al. 1980). Nearly all methods yield bonds that are too long by 1 – 3% (0.02 – 0.05 Å). The cc-pVDZ results are consistently 0.02 Å longer than those for the other basis sets. While Si-O bond lengths tend to approach the experimental value with each higher rung of

Jacob's ladder, the evolution is not monotonic. Of note are the M11-L/6-31G(d) and M11-L/def2-SVP methods, which appear to outperform all the others to yield average Si-O bond lengths within 0.002 Å of experiment.

Table 1. Average calculated Si-O bond lengths for the central SiO_2 tetrahedron. Experimental bond length is 1.608 Å (Levien et al. 1980).

		$\langle r_{Si\text{-}O} \rangle$ (Å)		
Method	**Type**	**6-31G(d)**	**cc-pVDZ**	**Def2-SVP**
BLYP	GGA	1.641	1.664	1.646
PBE	GGA	1.640	1.665	1.646
RevTPSS	Meta-GGA	1.638	1.663	1.643
M11-L	Meta-GGA	1.606	1.629	1.610
B3LYP	Hybrid GGA	1.628	1.651	1.634
PBE0	Hybrid GGA	1.625	1.649	1.631
M11	Hybrid meta-GGA	1.632	1.651	1.635
TPSSh	Hybrid meta-GGA	1.630	1.654	1.636

Table 2 compares the highest-frequency infrared-active mode to the highest-frequency transverse optical phonon mode (TO8) inferred from second-harmonic phonon spectroscopy for α-quartz (Winta et al. 2018). All the calculated harmonic frequencies are too low by as much as 9% (~100 cm^{-1}), with higher-level calculations generally performing better. The TPSSh functional is the only functional that does not follow this trend, although the total spread within a basis set is ~3% (30 – 40 cm^{-1}). Unlike for bond lengths, M11-L does not outperform the other methods on this arguably more important metric.

Table 2. Comparison of the strongest infrared-active harmonic vibrational frequencies calculated by DFT. Experimentally determined harmonic frequency is 1171 cm^{-1}.

		$\nu_{Si\text{-}O}$ (cm^{-1})		
Method	**Type**	**6-31G(d)**	**cc-pVDZ**	**Def2-SVP**
BLYP	GGA	1109	1072	1110
PBE	GGA	1109	1070	1111
RevTPSS	Meta-GGA	1118	1080	1121
M11-L	Meta-GGA	1120	1097	1137
B3LYP	Hybrid GGA	1144	1109	1144
PBE0	Hybrid GGA	1144	1114	1155
M11	Hybrid meta-GGA	1148	1121	1155
TPSSh	Hybrid meta-GGA	1134	1100	1139

Figure 7 compares the calculated quartz-SiO_2 fractionations from 0°C to 400°C. The spread in $^{18}O/^{16}O$ fractionation factors decreases as temperature increases, from 6 – 9‰ at 0°C to

~2‰ at 400°C. In contrast, the spread in $\theta^{eq}_{quartz-SiO_2}$ values is ~0.0005 over the entire temperature range. The cc-pVDZ basis set consistently predicts smaller $^{18}O/^{16}O$ fractionations (by ~2‰ at 0°C, on average) and higher $\theta^{eq}_{quartz-SiO_2}$ values. Disparities relative to the benchmark quartz-SiO_2 calculation range from 0.1 to 5‰ in $^{18}O/^{16}O$ fractionation at 0°C and are less than 0.0003 in $\theta^{eq}_{quartz-SiO_2}$ across the temperature range. Theory-observation agreement in vibrational frequencies was not a good predictor of the method-benchmark agreement in $^{18}O/^{16}O$ fractionation factor.

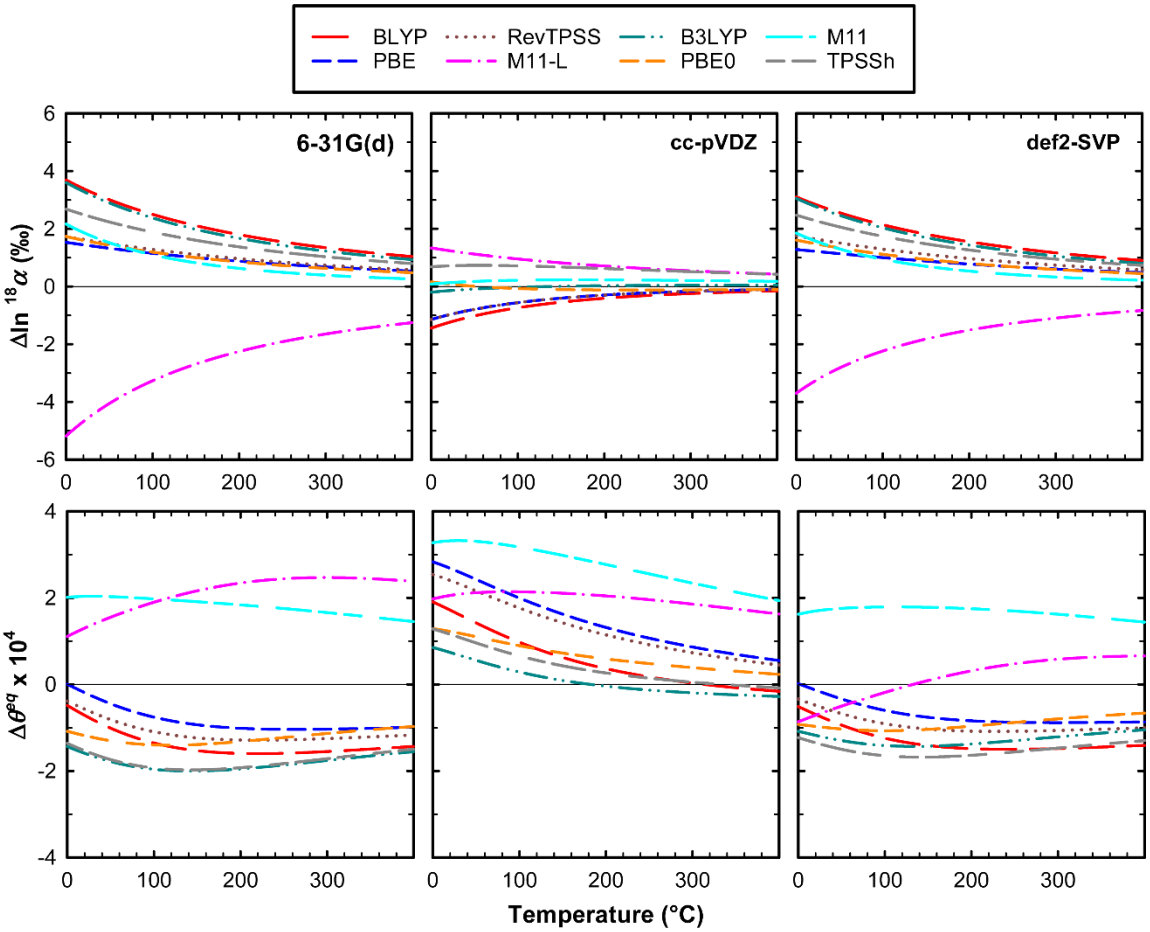

Fig. 7. Comparison of $^{18}O/^{16}O$ fractionation factors ($\Delta\ln^{18}\alpha = \ln^{18}\alpha_{calculated} - \ln^{18}\alpha_{benchmark}$) and θ^{eq} ($\Delta\theta^{eq} = \theta^{eq}_{calculated} - \theta^{eq}_{benchmark}$) for quartz-$SiO_{2(g)}$ equilibrium from 24 different electronic-structure method/basis set pairs.

We also evaluated how well these calculations objectively predict quartz-$H_2O_{(l)}$ fractionations based on the semi-empirical β^*- and κ-value fits for liquid water used in Hayles et al. (2018). The results show broadly similar trends as for quartz-$SiO_{2(g)}$ (Fig. 8). $^{18}O/^{16}O$ fractionations obtained from the cc-pVDZ basis set are consistently smaller than those from the 6-31G(d) and def2-SVP basis sets, with little difference in performance for $\theta^{eq}_{quartz-H_2O}$ values. Perhaps remarkably, our B3LYP/6-31G(d) calculation predicts a $^{18}O/^{16}O$ fractionation and $\theta^{eq}_{quartz-H_2O}$ value within 1.5‰ and 1 ppm, respectively, of the B3LYP/6-311G(d) benchmark across the temperature range; the basis set effect on θ appears to be negligible within the Pople

basis set family for this quartz cluster model. Both $^{18}O/^{16}O$ fractionations and $\theta^{eq}_{quartz-H_2O}$values systematically increase up the rungs on Jacob's ladder, amounting to a 10‰ range (~2‰ when omitting M11-L) at 0°C in $^{18}O/^{16}O$ fractionation and a 0.0007 range in $\theta^{eq}_{quartz-H_2O}$. The trends largely mirror the increase in the high-frequency mode with methodological complexity highlighted in Table 2, but the fractionation factors do not converge at high levels toward the benchmark calculation.

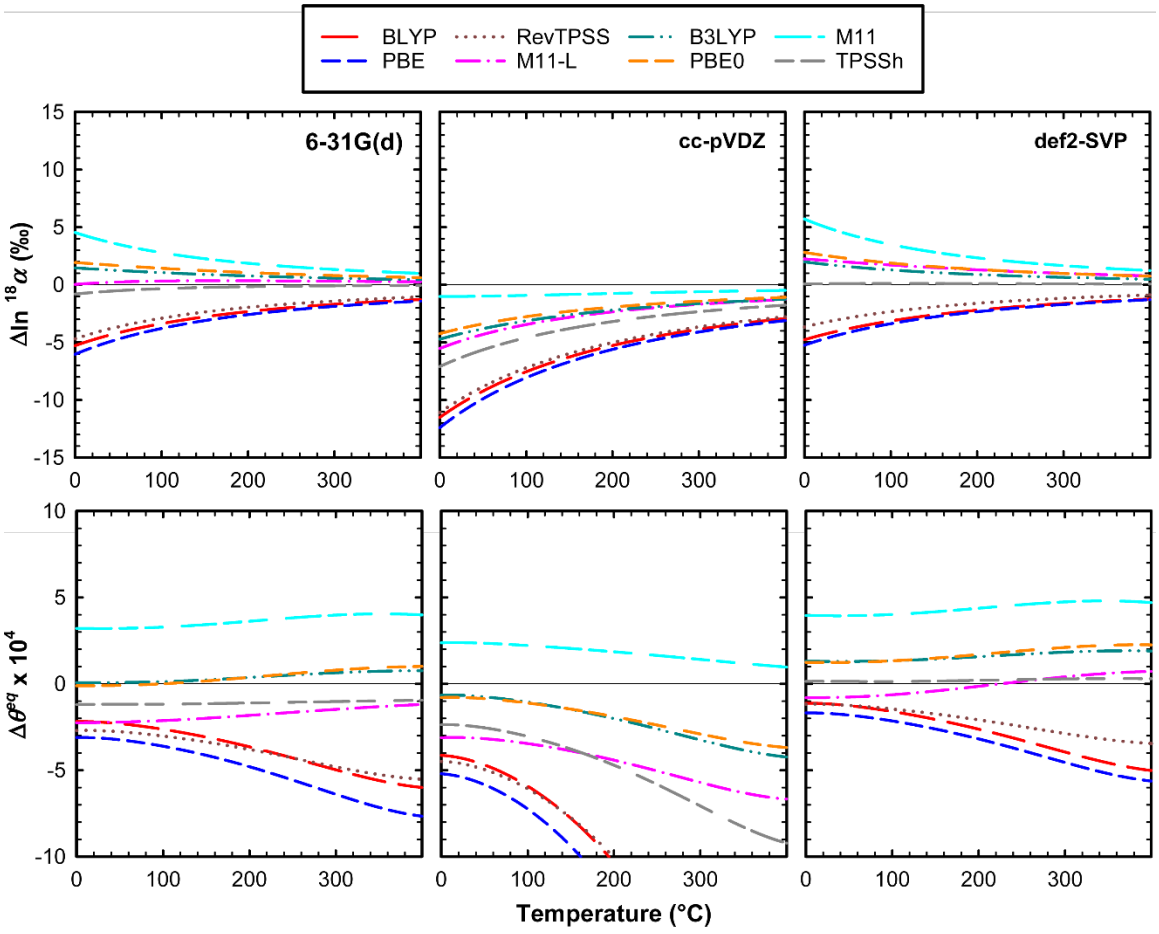

Fig. 8. Same as Figure 7, but for quartz-$H_2O_{(l)}$ fractionation derived from the fractionation factors of Hayles et al. (2018). Note the change in scale to encompass larger deviations from the benchmark calculation than in Figure 7.

Finally, we evaluated the effects of harmonic vibrational scaling using the scaling factors of Kesharwani et al. (2015). Frequencies for all isotopic species obtained from the calculations were uniformly scaled. Only a few combinations of theory and basis could be scaled, but general trends are still apparent; the results are shown in Figure 9. In this case, frequency scaling appears to mitigate much of the spread in $^{18}O/^{16}O$ fractionation associated with both the level of theory and the basis set size, although the final range of results is still ~3‰ in $^{18}O/^{16}O$ fractionation at 0°C. The method-to-method disparities in $\underline{\theta}$ values is also improved by about a factor of two. However, the B3LYP results deviate further from the benchmark upon scaling. We note that these empirically derived scaling factors depend strongly on both the molecular test set and

benchmarking method, so we consider this reduction in scatter between methods to be provisional.

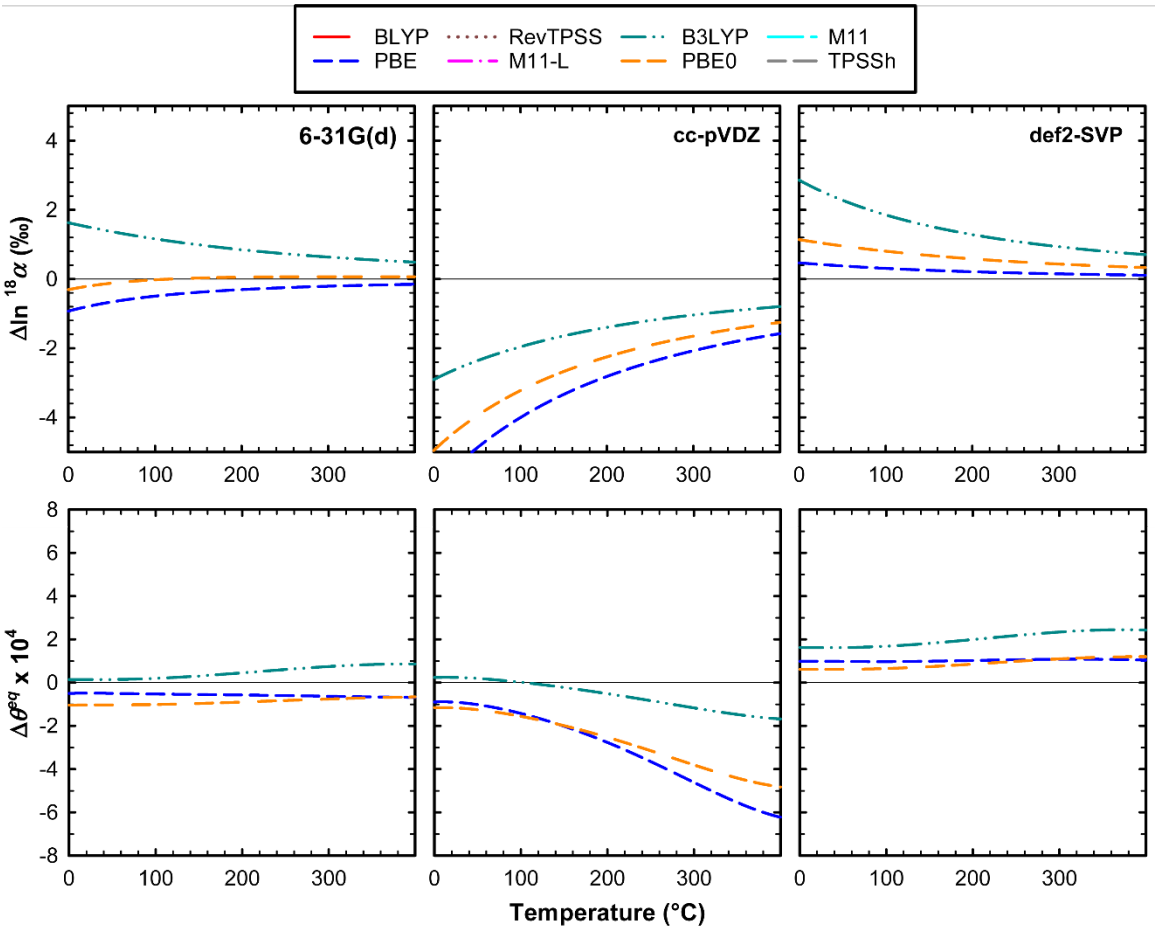

Fig. 9. Same as Figure 8, but after scaling vibrational frequencies according to empirical scaling factors. Note the change in scale reflecting improved agreement with the benchmark calculation relative to the unscaled calculations in Figure 8.

These results resemble those from another methodological intercomparison, made on oxyheme complexes relevant for triple-isotope effects in cellular respiration (Ash et al. 2020). Three functionals (GGA, hybrid GGA, and hybrid meta-GGA types) were used to investigate the triple-oxygen and clumped-isotope equilibrium isotope effects upon the binding of O_2 to a three different heme groups. The calculated $\theta_{\text{heme-O2}}$ values showed agreement within <0.001 at 25°C, but the calculated $^{18}O/^{16}O$ fractionations differed by as much as 8‰ at 25°C. While the varied change in bond strength upon binding drove the variable $^{18}O/^{16}O$ fractionations the mechanism of O-O bond weakening appeared to control the θ value.

Taken together, the most notable outcome of these comparisons is the insensitivity of θ to DFT method and basis set. The calculated $^{18}O/^{16}O$ fractionations are sensitive to the method used, and the systematic errors are insidious: merely changing the basis set can yield per-mil-level changes in predicted $^{18}O/^{16}O$ fractionations for a given molecular model. Fortuitous error cancellation appears to be limited to θ values, rendering them robust across methods and basis

sets. This relative invariance implies that θ values reflect something that is conserved between the approaches such as the nature and number of vibrational modes involving oxygen—which shift together upon an isotopic substitution—and/or their relative bond strengths. While the spread in raw calculated $^{18}O/^{16}O$ fractionations continues to be problematic, the use of literature harmonic vibrational frequency scaling factors may reduce disagreements among the theoretical methods, even when the geometries are slightly inaccurate. Using high-quality scaling factors, the accuracy of calculated equilibrium isotopic fractionation using inexpensive methods may be able to approach that of higher-level methods (in theory or basis set). If qualitative aspects of molecular vibrations and the *relative* harmonic frequencies remain accurate, the use of low-level DFT methods and small basis sets could provide useful insights into large molecular clusters (keeping in mind potential systematic errors, e.g., BSSE), although higher-level calculations may still be more accurate. Broadly, we expect that the accuracy of first-principles approaches does not yet exceed 2-3‰ in $^{18}O/^{16}O$ equilibrium fractionations and ~0.001 in θ values, but in many cases such accuracy is sufficient to advance the science and push the field into new areas.

ANALYTICAL CONSIDERATIONS

Boaz Luz and Eugeni Barkan led the group at Hebrew University first demonstrated the possibility of measuring oxygen triple-isotope compositions of natural materials to ultra-high precision (Luz et al. 1999; Luz and Barkan 2000; Barkan and Luz 2003; Luz and Barkan 2005). Their efforts first focused on atmospheric oxygen, but subsequent work demonstrated that ultra-high precision could be achieved for water as well (Barkan and Luz 2005; 2007; Luz and Barkan 2010; Affek and Barkan 2018). Improvements in measurements of CO_2 and mineral phases followed, owing to numerous analytical innovations (Hofmann et al. 2012b; Mahata et al. 2013; Pack et al. 2013; Levin et al. 2014; Pack and Herwartz 2014b; Passey et al. 2014; Barkan et al. 2015; Sharp et al. 2016; Laskar et al. 2019; Wostbrock et al. 2020) that include a new generation of optical isotope instruments (Berman et al. 2013; Steig et al. 2014; Prokhorov et al. 2019). State-of-the-art analytical precision is currently between 3 and 5 parts per million in $\Delta'^{17}O$ values.

Despite this high precision—which appears to be broadly achievable—significant inter-laboratory triple-isotope discrepancies have persisted. The most prominent of these may be the triple-isotope contrast between atmospheric O_2 and ocean water (Luz and Barkan 2011; Tanaka and Nakamura 2012; Young et al. 2014; Pack et al. 2017; Wostbrock et al. 2020). Labs measuring argon-free atmospheric O_2 consistently report smaller $\Delta'^{17}O$ differences, by up to 0.07‰. Similar disagreements exist in measurements of oxygen triple isotopes in carbonates (Passey et al. 2014; Barkan et al. 2015; Bergel et al. 2020; Voarintsoa et al. 2020; Wostbrock et al. 2020).

While the origins of these disagreements remain enigmatic, the discrepancies may be partially attributable to mass-spectrometric artifacts. One such artifact has been dubbed a "pressure baseline" (He et al. 2012; Yeung et al. 2018), any unwanted signal registering in the rare-isotope collection cups of a mass spectrometer that appear only when the analyte is present. They arise from positively or negatively charged isobars, and are especially pernicious in the

reference gas of a dual-inlet system: if the "true" reference ion current is different than what the instrument is registering, then the measured isotopic ratios will be inaccurate. The resulting scale distortion is usually non-mass-dependent because it is influenced by instrument geometry, ion-source conditions, and ion optics, and it disproportionately affects the weaker beams (i.e., $^{16}O^{17}O^{+}$ relative to $^{16}O^{18}O^{+}$).

Scale distortion and calibration

Yeung et al. (2018) derived a formula for a correction factor φ, which relates the (non-logarithmic) δ value to the relative size of the unwanted "pressure baseline" ion current (i_{BG}) and the intrinsic ion current due to the analyte (i_{ion}):

$$\delta^{\square}_{measured} = \frac{\delta^{\square}_{true}}{\left(1+\frac{i_{BG}}{i_{ion}}\right)_{REF}} = \varphi_{REF} \times \delta^{\square}_{true} \tag{20}$$

The φ factors for ^{17}O and ^{18}O-substituted analytes are typically neither equal nor mass-dependent, so they are related to the measured $\Delta'^{17}O$ value by the expression

$$\Delta'^{17}O_{measured} = \Delta'^{17}O_{true} + \ln\left(\frac{\varphi_{17,REF}}{\varphi_{17,SAM}}\right) - \lambda_{RL} \times \ln\left(\frac{\varphi_{18,REF}}{\varphi_{18,SAM}}\right) \tag{21}$$

It is important to notice that while φ_{REF} values are constant for a given reference gas and mass-spectrometric setting, the φ_{SAM} factor changes with isotopic composition, even if the pressure baseline is constant. The precise value of φ_{SAM} also depends on the abundance of the minor ion via i_{ion}. Therefore, because $\varphi_{REF} \neq \varphi_{SAM}$, this composition-dependent effect causes inaccuracies in measured $\Delta'^{17}O$ values. As the isotopic contrast between sample and reference gases becomes larger, so too does the difference between φ_{SAM} and φ_{REF}, and thus the $\Delta'^{17}O$ error. Measured λ values would thus be affected because the composition-dependent $\Delta'^{17}O$ error acts to "rotate" triple-isotope slopes (Fig. 10).

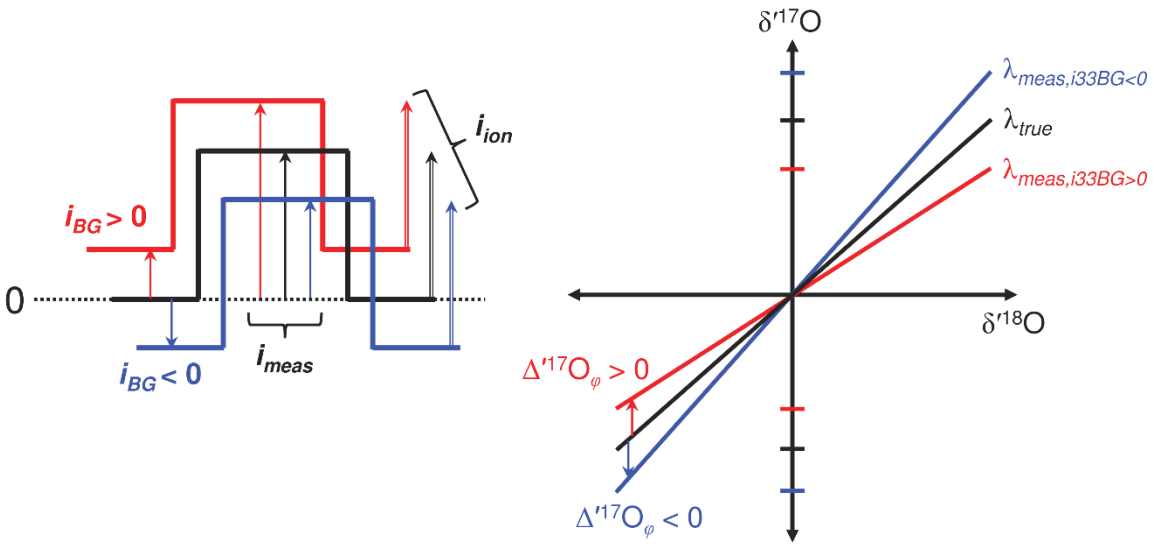

Fig. 10. Effect of mass-spectrometric pressure baselines on triple-isotope compositions. (Left) Schematic of positive and negative pressure baselines i_{BG}. (Right) Rotation of triple-isotope slopes, which alters observed λ values. Used by permission of John Wiley and Sons, from Yeung et al. (2018), *Rapid Commun. Mass Spectrom.*, Vol. 32, Figs. 1 and 3, p. 1813-1814.

How important is this effect? It can be significant. Consider a 1-V minor-isotope signal with a 1-mV pressure baseline being reported by a 10^{11}-Ω amplifier, which is in the range of what has been observed before (Yeung et al. 2012; Young et al. 2014; Yeung et al. 2018). In that case, i_{BG} = 10 fA with i_{ion} = 10 pA, resulting in φ_{REF} = 0.999. A sample with the same i_{BG} but δ_{true} = +20‰ would thus yield $\delta_{measured}$ = 19.98‰, a deviation of -20 ppm from the true value. If δ_{true} = +40‰, then $\delta_{measured}$ = 39.96‰ and the deviation is -40 ppm. Such an error would typically be regarded as insignificant for $\delta^{18}O$ values, but it is significant for $\Delta'^{17}O$ values. The error is comparable to the difference between bulk silicate earth and seawater in $\Delta'^{17}O$ values (Pack et al. 2016) and would result in a measured λ value that is too shallow by ~0.001. In a field where scientific conclusions are routinely based on ppm-level composition differences and slope differences of 0.001 – 0.005, this otherwise subtle effect becomes quite a nuisance if gone unnoticed. Furthermore, the problem can become more significant and more difficult to correct when sample and reference gases have different amounts of a major isobar (e.g., argon in O_2).

Some triple-isotope analysts have independently solved the problem of inter-laboratory agreement by tying isotopic measurements to a two-point (e.g., VSLAP2-VSMOW2), rather than single-point calibration scale (Berman et al. 2013; Schoenemann et al. 2013). The two-point scale implicitly allows the analyst to determine φ_{REF} values, which are equivalent to oft-used empirical "stretching" factors. The greatest accuracy is achieved when the two calibration tie-points show a large difference in isotopic composition (e.g., 55.5‰ for VSLAP2-VSMOW2); measurements of water triple isotopes across three labs showed agreement within 8 ppm using this method, in spite of the different techniques utilized (Berman et al. 2013). Note, however, that the two materials used for triple-oxygen calibration need to have a large and known (or at least agreed-upon) isotopic contrast, preferably >20‰ in $\delta^{18}O$ value. Two calibrated laboratory working gases differing in isotopic composition could serve the same purpose with a significantly reduced analytical burden.

We will note that the VSMOW-VSLAP scale for triple-oxygen measurements is currently assigned rather than objectively known. The λ = 0.528 value relating the two standards is merely an accepted value; a difference between the accepted value of λ and the objectively true value would result in a scale distortion in the VSMOW-VSLAP scale, and disagreements between theoretical and experimental values of triple-isotope fractionation.

In practice, these considerations likely limit the accuracy of reported triple-isotope differences to ±10 ppm, and observed λ values to ±0.001, even when labs are well calibrated and despite higher intra-laboratory precision. While the magnitude of these potential errors is worth estimating independently in every laboratory, we caution against over-interpreting signals within these uncertainty ranges, especially when the interpretations rely on assumed inter-laboratory agreement. Reporting isotopic compositions using traceable, multi-point standardization procedures will also aid in improving data quality in future compilations.

Physical and reservoir effects in the real world

Isotopic signals of interest, of course, are seldom as simple as to be limited by theoretical or analytical uncertainties in nature. Atoms in molecules often arrive at mineral or complex through a convoluted physical path, fractionated from their source reservoir, and perhaps mixed with atoms from other sources. Examples relevant to the triple-oxygen system include the evaporation, condensation, diffusion, and mixing of water vapor or the interphase transfer of CO_2 and O_2 (Schoenemann and Steig 2016; Guo and Zhou 2019; Li et al. 2019). The theory of mass-dependent fractionation includes descriptions of these predominantly physical effects (here loosely defined as those that do not involve bond breaking or structural distortion). These effects cause subtle, but meaningful isotopic effects that overprint the intrinsic chemical effects calculated by first-principles methods.

It is well known that two-endmember reservoir mixing yields curved trajectories in a cross-plot of $\Delta'^{17}O$ vs. $\delta'^{18}O$ because $\Delta'^{17}O$ values are defined on a logarithmic scale (Miller 2002). Consider the contamination of an oxygen-isotope reservoir by a secondary source that differs by 30‰ in $\delta'^{18}O$, but has the same $\Delta'^{17}O$ value: just a 10% contamination in this case is needed to cause a ~10 ppm $\Delta'^{17}O$ depletion relative to the pure reservoir. Smaller $\delta'^{18}O$ differences between reservoirs yield smaller $\Delta'^{17}O$ deviations. Thus the presence of secondary phases in various materials needs to be evaluated explicitly when interpreting measurements at or near the limits of analytical precision. For example, quartz derived from silica diagenesis may lead to heterogeneity at the sum-millimeter scale, which would lower $\Delta'^{17}O$ values relative to diagenetic quartz with the same $\delta'^{18}O$ value crystallized at a single, well-defined temperature (Marin-Carbonne et al. 2012; Stefurak et al. 2015; Sengupta and Pack 2018; Hayles et al. 2019; Liljestrand et al. 2020). In marine dissolved-oxygen studies, the presence of unusually low $\Delta'^{17}O$ values at low oxygen concentrations has also been attributed to mixing (Hendricks et al. 2005; Nicholson et al. 2014), although they may also be due to biological or analytical artifacts (Stolper et al. 2018; Yeung et al. 2018; Ash et al. 2020).

Other physical effects such as molecular diffusion can be important as well. They overprint intrinsic chemical isotope effects in both geochemical and biogeochemical systems. In the gas phase, the triple- and multi-isotopologue effects of diffusion in a variety of molecules can be calculated with high accuracy using the kinetic theory of gases (Eiler and Schauble 2004; Barkan and Luz 2007; Yeung et al. 2012; Magyar et al. 2016; Yeung et al. 2017; Li et al. 2019): the fractionation factor in a non-interacting gas mixture is determined by the reduced mass of the diffuser and the medium by the relation $\alpha = (\mu/\mu^*)^{1/2}$, where the asterisk indicates that the isotopically substituted diffuser is used in the reduced mass calculation. For example, a calculation for O_2 diffusing through N_2 yields ${}^{18}\alpha = 0.986$ and $\theta = 0.513$. The one published experiment on this process showed ${}^{18}\alpha = 0.9849 \pm 0.0001$ and $\theta = 0.5228 \pm 0.0002$ (1σ) instead (Angert et al. 2003), indicating some experimental or analytical bias. Experiments on the diffusive fractionation of water vapor through air yielded better agreement, with ${}^{18}\alpha = 0.9725 \pm 0.0003$ and $\theta = 0.5185 \pm 0.0002$ (1σ), while theory predicts ${}^{18}\alpha = 0.969$ and $\theta = 0.519$ (Barkan and Luz 2007). The above approach may not be valid for a diffuser and medium that interact meaningfully with each other (e.g., SO_2 in water vapor), but there have been few investigations related to these systems; an analogue to such systems might be gas-solid interaction, which are known to cause unusual isotope effects at low temperatures (Eiler et al. 2013).

Aqueous-phase diffusive isotope effects are therefore less straightforward to calculate; solute-solvent interactions are generally significant enough to merit a revision to the simple

ideal-gas reduced-mass power law. For example, the kinetic mass dependence of noble gases diffusing through water deviates strongly from $(\mu/\mu^*)^{1/2}$ for atoms larger than He; however, the limited data on multi-isotope trends is inconclusive as to whether θ values are anomalous (Bourg and Sposito 2008; Tyroller et al. 2014; Tyroller et al. 2018; Seltzer et al. 2019). While experimentally determined $\Delta'^{17}O$ and clumped-isotope fractionations for molecular oxygen diffusion are consistent with the reduced-mass power law above, the $^{18}O/^{16}O$ fractionation indicates that exponent is either smaller (0.2) or the characteristic diffusion partner has a larger mass (e.g., corresponding to several water molecules) (Knox et al. 1992; Li et al. 2019). Diffusion of charged species is strongly affected by the energetic cost of ion desolvation, lowering their effective exponent as well (Richter et al. 2006; Bourg et al. 2010; Hofmann et al. 2012a). Consequently, diffusive isotope effects manifest in many crystal growth environments (Watkins et al. 2017), resulting in diffusion-influenced $^{18}\alpha$ and θ values in real systems.

To illustrate the importance of diffusive fractionation on more "typical" geochemical processes, consider a two-step reaction that has a reversible first step and an irreversible second step:

$$A \rightleftharpoons B \rightarrow C$$

This scheme has been used to describe CO_2 fixation by leaves (O'Leary 1981), respiratory oxygen consumption (Stolper et al. 2018; Ash et al. 2020), and mineral precipitation (Watkins et al. 2014; Watkins et al. 2017), among many others. In all of these cases, molecular diffusion is the first reversible step, although the physical processes are slightly different (e.g., gas-phase, in and out of leaves through stomata vs. aqueous phase, through the crystallizing boundary layer). Assuming that the reaction proceeds keeping B in steady state, one can show that the effective fractionation factor α_{eff} and exponent θ_{eff} for A is (Bao et al. 2015):

$$\alpha_{eff} = \frac{\alpha_1}{r\left(\frac{\alpha_1}{\alpha_2}\right) + 1 - r} \tag{22}$$

$$\theta_{eff} = \ln \frac{{}^{17}\square\alpha_1 - ¿ \ln\left[r\left(\frac{{}^{17}\square\alpha_1}{{}^{17}\square\alpha_2}\right) + 1 - r\right]}{\ln {}^{18}\square\alpha_1 - ¿ \ln\left[r\left(\frac{{}^{18}\square\alpha_1}{{}^{18}\square\alpha_2}\right) + 1 - r\right]¿} \tag{23}$$

where r is the reversibility of $A \rightleftharpoons B$, defined as the flux $B \rightarrow A$ divided by the flux $A \rightarrow B$, with $r = 1$ for equal fluxes. Diffusion limitation of reactions can therefore drive $^{18}\alpha_{eff}$ and θ_{eff} values toward those characteristic of diffusion, which are typically smaller than those for equilibrium crystallization. Moreover, one may be tempted to infer that θ_{eff} always lies in between that for each step, θ_1 and θ_2, function of r. However, the equation predicts non-monotonic variations when θ_1 is similar to θ_2 and when the $^{18}\alpha_1$ and $^{18}\alpha_2$ are quite different (Fig. 11).

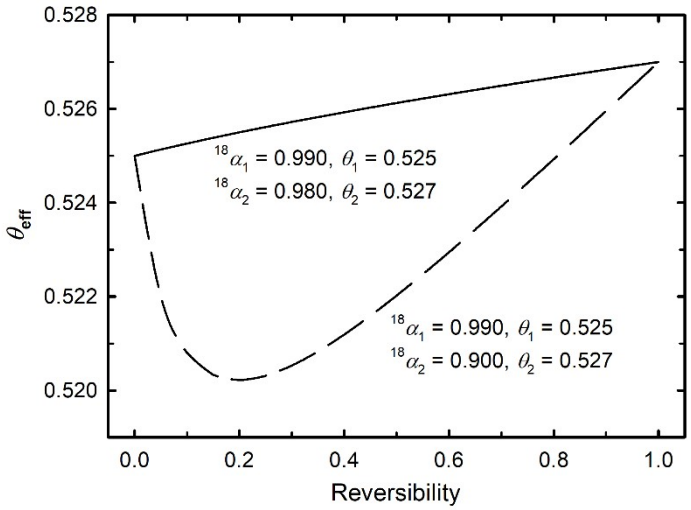

Fig. 11. Monatonic and non-monatonic trends in θ_{eff} for a two-step reaction according to eqn. (23). The upper curve corresponds to processes with similar $^{18}O/^{16}O$ fractionation factors, while the lower curve corresponds to processes with different $^{18}O/^{16}O$ fractionation factors, all else unchanged.

CASE STUDY: KINETIC ISOTOPE FRACTIONATION DURING CARBONATE ACID DIGESTION

The transformation of carbonate minerals into CO_2 analytes is most commonly achieved via phosphoric acid digestion (McCrea 1950). During this process, only two of the three C-bound oxygen atoms are preserved in CO_2, resulting in a kinetic isotope fractionation. This reaction has been studied extensively, both experimentally and theoretically, for $^{18}O/^{16}O$ as well as triple-oxygen and clumped isotope fractionation to aid in the reconstruction of the original carbonate isotopic composition (Kim and O'Neil 1997; Kim et al. 2007; Guo et al. 2009; Passey et al. 2014; Müller et al. 2017; Petersen et al. 2019; Swart et al. 2019; Bergel et al. 2020; Wostbrock et al. 2020; Zhang et al. 2020). Yet, despite the considerable efforts of the community, the isotopic fractionation factors remain uncertain. We will use this as a case study of theory versus the "real world," focusing on triple oxygen isotopes.

The problems

Two transition-state theory investigations of triple-isotope trends in the reaction have been published, both using the B3LYP level of theory. Guo et al. (2009) used the double-zeta 6-31G(d) basis set to investigate H_2CO_3 hydrolysis and dehydroxylation, whereas Zhang et al. (2020) used the triple-zeta basis set with diffuse functions 6-311G+(d,p) to investigate H_2CO_3-catalyzed, H_3O^+-catalyzed, and H_3PO_4-catalyzed mechanisms for H_2CO_3 decomposition (Fig. 12). Both investigations scaled the B3LYP vibrational frequencies to those obtained from higher-level wavefunction methods (MP2 and coupled-cluster, respectively). These calculations yielded

θ^{kin}_{acid} values between 0.525 and 0.529 at 25°C, depending on the mechanism, with an effective θ^{kin}_{acid} of 0.528 and 0.527, respectively. In contrast, the calculated $^{18}O/^{16}O$ fractionation factors are different by 0.5‰ at room temperature, with ln $^{18}\alpha_{acid}$ = 10.7‰ and 10.2‰, respectively. Experimental studies have yielded $^{18}O/^{16}O$ fractionation factors within this range (Kim and O'Neil 1997; Kim et al. 2007). Guo et al. (2009) noted some variability arising from the carbonate partner cation and crystal structure. Zhang et al. attribute the spread in experimental $^{18}O/^{16}O$ fractionation factors to partial hydration of nominally anhydrous ortho-phosphoric acid, which increases the proportion of carbonate reacting through the H_3O^+-catalyzed pathway.

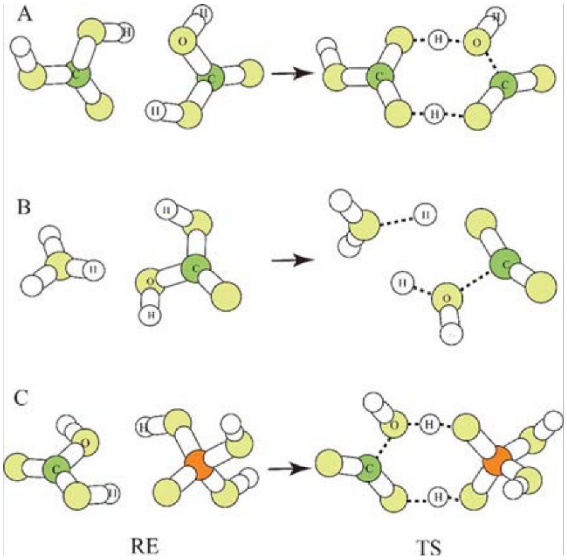

Fig. 12. Three relevant reactants (RE) and transition states (TS) for carbonic acid decomposition during acid digestion of carbonates. Shown are structures for the (A) H_2CO_3-catalyzed, (B) H_3O^+-catalyzed, and (C) H_3PO_4-catalyzed pathways. Used by permission of ACS Publications, from Zhang et al. (2020), *ACS Earth Space Chem.*, Vol. 4, Fig. 1, p. 422.

The two published experimental measurements of θ^{kin}_{acid} disagree with both the theoretical calculations and with each other. The most direct determination of θ^{kin}_{acid} was by Wostbrock and Sharp (2019), who bomb-fluorinated three calcite standards (NBS-18, NBS-19/19a, and IAEA-603) and the CO_2 liberated through acid digestion of that standard. Across all three standards, they reported consistent θ^{kin}_{acid} values of 0.523 using this method after standardizing against VSMOW2 and VSLAP2 using direct BrF_5 fluorination of those waters. Bergel et al. (2020) determined θ^{kin}_{acid} indirectly using their determinations of (1) the $\Delta'^{17}O$ values in CO_2 liberated from biogenic molluskan aragonite that had presumably grown at equilibrium at constant temperatures and (2) the $\Delta'^{17}O$ values of water samples in which the mollusks grew. These two quantities were used to obtain an effective θ value between carbonate-derived CO_2 and water. Using this quantity and independently determined θ^{eq} values for carbonate-water equilibrium from theory ($\theta^{eq}_{carbonate-H_2O}$ = 0.526) (Guo et al. 2009; Hayles et al. 2018) or experiment [0.525; (Gibbons et al. 2017)], the value of θ^{kin}_{acid} was inferred to be 0.516 or 0.517. Voarintsoa et al. (2020) also found similar results for inorganically precipitated laboratory calcite. Like the measurements of Wostbrock and Sharp (2019), these measurements, too, were standardized to

VSMOW and VSLAP through two laboratory working standards (Barkan and Luz 2005; Affek and Barkan 2018).

Evaluation of theory and measurements

First, we will evaluate the theoretical prediction of θ_{acid}^{kin}. One could question the accuracy of B3LYP calculations for predicting accurate transition-state structures (Xu et al. 2011), which would affect the predicted kinetic isotope effects. However, both calculations yielded transition-state structures that compared favorably with high-level wavefunction-theory based structures and energies, which are reasonably accurate; moreover, the vibrational frequencies of the transition states were scaled to harmonic frequencies obtained from the wavefunction methods. Given these accuracy checks, and the relative insensitivity of calculated θ values to method and basis set, we do not believe that electronic structure methodology is a significant source of systematic error for θ values. However, both studies derive isotopic fractionations for acid digestion using the following simplifying assumptions: (*i*) the reaction occurs in the gas phase and (*ii*) the first step of the process—carbonate ion protonation—exhibits no isotopic effects. The bias introduced by the first assumption is difficult to assess, but surface and/or solvent stabilization almost certainly plays a role in the reaction pathway. The transition state, and this the kinetic isotope effect, will likely be affected. Regarding the latter assumption, the three oxygen positions are not chemically identical; only two of the three oxygens are protonated in a reacting H_2CO_3 molecule. Thus a site-specific protonation isotope effect could be relevant, one that biases the initial isotopic composition of the H-bound oxygens in H_2CO_3.

Both theory and experiment suggest that surface hydrolysis of calcite by water exposes $Ca(OH)(HCO_3)$ species, which reacts with acid to form the H_2CO_3 that decomposes to CO_2 and H_2O (Stipp et al. 1994; Kuriyavar et al. 2000; Al-Hosney and Grassian 2004). As a two-step reaction with a reversible protonation by the acid HX, the process could be represented schematically by:

$$Ca(OH)(HCO_3) + HX \rightleftharpoons Ca(OH)X + H_2CO_3 \rightarrow CO_2 + H_2O$$

with the H_2CO_3 decomposition proceeding through any of the pathways previously investigated. The protonation step may consist of two elementary steps, i.e., $CO_3^{2-} + H^+$ and $HCO_3^- + H^+$, but we will assume that these steps yield a net isotopic fractionation α_H. Using eqn. (23), the effective θ^{kin} value is therefore:

$$\theta_{acid,eff}^{kin} = \ln \frac{{}^{17}_{\square}\alpha_H - ¿ \ln\left[r\left(\frac{{}^{17}_{\square}\alpha_H}{{}^{17}_{\square}\alpha_{decomp}} \right) + 1 - r \right]}{\ln {}^{18}_{\square}\alpha_H - ¿ \ln\left[r\left(\frac{{}^{18}_{\square}\alpha_H}{{}^{18}_{\square}\alpha_{decomp}} \right) + 1 - r \right] ¿} ¿$$

A θ value for the first step less than 0.527 could lower $\theta_{acid,eff}^{kin}$ significantly from the acid-digestion-only value if protonation is not completely reversible (i.e., $r < 1$). However, a $\theta_{acid,eff}^{kin}$ value of 0.516 – 0.517 is difficult to explain. One way to display such low $\theta_{acid,eff}^{kin}$ values is for

the associated pathway to involve essentially no oxygen-isotope vibrations beyond the reaction coordinate. However, the presence of three potential oxygen-isotope substitutions on H_2CO_3 implies that other pathways contribute to the mean θ^{kin}_{acid} value for H_2CO_3 decomposition. Another possibility would be for H_2CO_3 decomposition to be near an isotope-effect crossover at room temperature. However, the measured $^{18}O/^{16}O$ fractionation for acid digestion is relatively large (10‰), suggesting that the reaction does not have a crossover in this temperature range. A third possibility is that the mechanisms have the right combination of vibrational modes in the transition states to express these kinetic isotope effects, but that is disfavored by the DFT calculations. Consequently, while $\theta^{kin}_{acid,eff} < 0.527$ is plausible, a value as low as 0.516 appears improbable. Nevertheless, the molecular model of the reaction used in theoretical investigations deserves additional scrutiny; the simplifying assumptions may not be sufficiently accurate to describe the acid digestion process.

We now turn our attention to the disagreement between laboratory determinations of θ^{kin}_{acid}. Clearly, the results ($\theta^{kin}_{acid} = 0.523$ and $0.516 – 0.517$) cannot both be correct; the origin of the discrepancy likely lies in the differences in methodology. The bomb-fluorination method of Wostbrock and Sharp (2019) yielded poorer reproducibility in $\delta^{18}O$ values (e.g., exceeding ±1‰ for NBS-19/19a) but good reproducibility in $\Delta'^{17}O$ values, resulting in an uncertainty in the carbonate-CO_2 $\Delta'^{17}O$ difference of about 16 – 24 ppm (i.e., the half-width of 95% confidence interval is 8 – 12 ppm). This conservative estimate of the random errors yields an uncertainty of ±0.002 in that determination of θ^{kin}_{acid}. The indirect determination of θ^{kin}_{acid} by Bergel et al. (2020) has less well constrained uncertainties given that it utilizes a mix of experimental and theoretical results. Assuming an overall uncertainty of about ±0.001 in each θ value used to derive θ^{kin}_{acid} indirectly also yields a likely uncertainty of ±0.002 in that determination. The results are still significantly different; what other methodological differences are relevant?

The measurements are both standardized using VSMOW and VSLAP, but each lab does so slightly differently. First, the method for analyzing the $\Delta'^{17}O$ value of water is different between labs: the University of New Mexico (UNM) group uses direct BrF_5 fluorination of water in a nickel micro-bomb to make an O_2 analyte, while the Hebrew University group uses CO_2-H_2O exchange followed by CO_2-O_2 exchange on a platinum sponge at 750°C to make their O_2 analyte (Barkan et al. 2015; Affek and Barkan 2018). The latter double-exchange method allowed both the carbonate and its growth water to be measured as O_2, limiting potential errors relating to standardizing different analytes. Affek and Barkan (2018) showed that it could reproduce data obtained from CoF_3 fluorination of water within analytical precision once normalized on the VSMOW-VSLAP scale. Second, Wostbrock and Sharp (2019) report isotopic compositions relative to VSMOW, eschewing the use of normalizing factors (Schoenemann et al. 2013), and obtain $\Delta'^{17}O = –15 \pm 7$ ppm (95% CI) for VSLAP. The absence of normalizing factors is justified because their reported $\delta^{18}O$ value for VSLAP is nearly identical to the IAEA recommended value (–55.5‰), although we note that the absence of scale distortion for $\delta^{18}O$ values does not imply an absence for $\delta^{17}O$ values. The Hebrew University group report isotopic compositions on the VSMOW-VSLAP scale, but it is not clear whether normalizing factors were used; they report $\Delta'^{17}O = 7 \pm 5$ ppm (95% CI) for SLAP, but their reported $\delta^{18}O$ value (–55.1‰) is slightly higher than the IAEA recommended value (Barkan and Luz 2005; Luz and Barkan 2010). This difference of 22 ± 9 ppm (95% CI) resembles the disparity between labs in the

measurement of NBS-19/19a and NBS-18: the UNM group report a $\Delta'^{17}O$ difference of 54 ± 17 ppm (95% CI), whereas the Hebrew University group most recently reported a $\Delta'^{17}O$ difference of 16 ± 6 ppm (95% CI) (Barkan et al. 2019); the offset between these measurements is 38 ± 18 ppm (95% CI).

Noting that the difference in $\delta^{18}O$ value between NBS-19/19a and NBS-18 (21.45‰) is twice that for acid digestion (10.2‰), the results are consistent with a scaling inconsistency between the two labs, with UNM-measured θ values being ~0.002 higher than those derived from the Hebrew University group. Therefore, once normalized on the VSMOW-VSLAP scale and using conservative estimates for random errors, the θ^{kin}_{acid} discrepancy becomes much smaller (0.523 ± 0.002 vs. 0.518 – 0.519 ± 0.002). A downward revision of the theoretically predicted $\theta^{kin}_{acid,eff}$ value after inclusion of the carbonate protonation step may bring theory and experiment into closer agreement, although the experimental θ^{kin}_{acid}value continues to be lower.

We therefore hypothesize that the theory-experiment disagreement in θ^{kin}_{acid} arises partially from an oversimplification of the molecular mechanism of acid digestion and partially from inconsistent laboratory standardization. Transition-state theory argues against $\theta^{kin}_{acid} = 0.516$, but multi-step acid digestion chemistry suggests that the effective value may be less than 0.527, and the effects of surface and/or solvent stabilization are unknown. Additional theoretical calculations are therefore needed to evaluate the veracity of the theoretical model. Even more exacting experiments, wherein the 95% confidence limits of θ^{kin}_{acid} can be reduced at least by a factor of two, will be needed to obtain a higher-precision comparison with theory. Emerging laser-based techniques will offer a useful test of analytical biases of these measurements (Berman et al. 2013; Steig et al. 2014; Prokhorov et al. 2019)

CONCLUDING REMARKS

A central challenge in theoretical isotope geochemistry has been to calculate isotopic fractionation with sufficient accuracy to predict, validate, and/or extend the useful range of experimental studies. In oxygen triple isotopes, the challenge is more acutely focused because the isotopic variations of interest are often near limits of analytical and theoretical accuracy. At present, it appears that theory and observations are well matched, with comparable uncertainties that allow one to push the other forward. However, we argue that these uncertainties are generally underestimated—by twofold or more—owing to cryptic systematic biases in both theory and measurements that have only recently to light. Geochemical triple-isotope mass-balance models seldom propagate these more realistic uncertainties forward.

Improving triple-oxygen analysis beyond its present level of accuracy will require more than just a sustained effort to understand and correct for these remaining sources of systematic errors. With higher precision and accuracy comes higher detail and potentially a new set of problems, including ever more subtle expressions of chemical, physical, and reservoir effects in natural systems. This dilemma is not unlike the task of measuring the length of a coastline (a problem made famous by Benoit Mandelbrot).

However, we contend that DFT-based isotopic calculations are still underutilized in the isotope geochemist's toolkit. They are now affordable for a wide range of geochemically interesting systems, including large and solvated molecular clusters, for triple-isotope analysis and beyond. The fortuitous cancellation of errors for multi-isotope fractionation trends, combined with the potential effectiveness of empirical harmonic frequency scaling factors allows DFT to bring first-order insights to oxygen triple-isotope fractionation even on a desktop computer using open-source software. For example, the pathways for isotopic fractionation associated with incorporating small atmospheric $\Delta'^{17}O$ signatures into minerals through weathering and biological cycling have not been rigorously investigated, despite their importance for triple-oxygen-based CO_2 paleobarometry (Kohn 1996; Bao et al. 2008; Kohl and Bao 2011; Pack et al. 2013; Passey et al. 2014; Bao 2015; Crockford et al. 2018; Waldeck et al. 2019; Sutherland et al. 2020).

In addition, few triple-isotope fractionation studies have been conducted for open-shell systems, which not only include free-radical reactions relevant to the atmospheric chemistry, but also many interesting reactions in biochemistry. The sensitivity to electronic structure calculation methods highlighted above is heightened in those systems, as improper accounting of electron spin, stabilizing long-range interactions, and basis-set biases can lead to qualitative errors in chemical structures and (presumably also) derived partition functions. Nevertheless, a judicious choice of methods and some chemical intuition may bring new insight to oxygen cycling and new predictions for geochemical tracers that can be tested by measurements.

ACKNOWLEDGEMENTS

This work was supported by the David & Lucile Packard Foundation Science and Engineering Fellowship to L. Y. Y. and National Science Foundation Postdoctoral Fellowship (grant EAR-1806124) to J. A. H.

REFERENCES

Abe O (2008) Isotope fractionation of molecular oxygen during adsorption/desorption by molecular sieve zeolite. Rapid Commun Mass Spectrom 22, doi:10.1002/rcm.3634

Adamo C, Barone V (1999) Toward reliable density functional methods without adjustable parameters: The PBE0 model. J Chem Phys 110:6158-6170, doi:10.1063/1.478522

Affek HP, Barkan E (2018) A new method for high-precision measurements of $^{17}O/^{16}O$ ratios in H_2O. Rapid Commun Mass Spectrom 32:2096-2097, doi:10.1002/rcm.8290

Al-Hosney HA, Grassian VH (2004) Carbonic Acid: An Important Intermediate in the Surface Chemistry of Calcium Carbonate. J Am Chem Soc 126:8068-8069, doi:10.1021/ja0490774

Angert A, Cappa CD, DePaolo DJ (2004) Kinetic ^{17}O effects in the hydrologic cycle: Indirect evidence and implications. Geochim Cosmochim Acta 68:3487-3495

Angert A, Rachmilevitch S, Barkan E, Luz B (2003) Effects of photorespiration, the cytochrome pathway, and the alternative pathway on the triple isotopic composition on atmospheric O_2. Global Biogeochem Cycles 17:1030

Ash JL, Yeung LY, Hu H (2020) What fractionates oxygen isotopes during respiration? Insights from multiple isotopologue measurements and theory. ACS Earth and Space Chemistry 4:50-66, doi:10.1021/acsearthspacechem.9b00230

Babikov D, Kendrick BK, Walker RB, Pack RT (2003) Formation of ozone: Metastable states and the anomalous isotope effect. J Chem Phys 119:2577-2589
Baker L, Franchi IA, Maynard J, Wright IP, Pillinger CT (2002) A Technique for the Determination of $^{18}O/^{16}O$ and $^{17}O/^{16}O$ Isotopic Ratios in Water from Small Liquid and Solid Samples. Anal Chem 74:1665-1673, doi:10.1021/ac010509s
Balan E, Cartigny P, Blanchard M, Cabaret D, Lazzeri M, Mauri F (2009) Theoretical investigation of the anomalous equilibrium fractionation of multiple sulfur isotopes during adsorption. Earth Planet Sci Lett 284:88-93, doi:https://doi.org/10.1016/j.epsl.2009.04.010
Bao H (2015) Sulfate: A time capsule for Earth's O_2, O_3, and H_2O. Chem Geol 395:108-118, doi:https://doi.org/10.1016/j.chemgeo.2014.11.025
Bao H, Lyons JR, Zhou C (2008) Triple oxygen isotope evidence for elevated CO_2 levels after a Neoproterozoic glaciation. Nature 453:504-506, doi:10.1038/nature06959
Bao H, Cao X, Hayles JA (2015) The confines of triple oxygen isotope exponents in elemental and complex mass-dependent processes. Geochim Cosmochim Acta 170:39-50, doi:http://dx.doi.org/10.1016/j.gca.2015.07.038
Bao H, Cao X, Hayles JA (2016) Triple Oxygen Isotopes: Fundamental Relationships and Applications. Annu Rev Earth Planet Sci 44:463-492, doi:10.1146/annurev-earth-060115-012340
Barkan E, Luz B (2003) High-precision measurements of $^{17}O/^{16}O$ and $^{18}O/^{16}O$ of O_2 and O_2/Ar ratio in air. Rapid Commun Mass Spectrom 17:2809-2814
Barkan E, Luz B (2005) High precision measurements of $^{17}O/^{16}O$ and $^{18}O/^{16}O$ ratios in H_2O. Rapid Commun Mass Spectrom 19:3737-3742
Barkan E, Luz B (2007) Diffusivity fractionations of $H_2{}^{16}O/H_2{}^{17}O$ and $H_2{}^{16}O/H_2{}^{18}O$ in air and their implications for isotope hydrology. Rapid Commun Mass Spectrom 21:2999-3005, doi:doi:10.1002/rcm.3180
Barkan E, Musan I, Luz B (2015) High-precision measurements of $\delta^{17}O$ and $^{17}O_{excess}$ of NBS19 and NBS18. Rapid Commun Mass Spectrom 29:2219-2224, doi:10.1002/rcm.7378
Barkan E, Affek HP, Luz B, Bergel SJ, Voarintsoa NRG, Musan I (2019) Calibration of δ17O and 17Oexcess values of three international standards: IAEA-603, NBS19 and NBS18. Rapid Commun Mass Spectrom 33:737-740, doi:10.1002/rcm.8391
Becke AD (1993) Density-functional thermochemistry. III. The role of exact exchange. J Chem Phys 98:5648-5652, doi:10.1063/1.464913
Becke AD (2014) Perspective: Fifty years of density-functional theory in chemical physics. J Chem Phys 140:18A301, doi:10.1063/1.4869598
Bergel SJ, Barkan E, Stein M, Affek HP (2020) Carbonate $^{17}O_{excess}$ as a paleo-hydrology proxy: Triple oxygen isotope fractionation between H_2O and biogenic aragonite, derived from freshwater mollusks. Geochim Cosmochim Acta 275:36-47, doi:https://doi.org/10.1016/j.gca.2020.02.005
Bergquist BA, Blum JD (2007) Mass-Dependent and -Independent Fractionation of Hg Isotopes by Photoreduction in Aquatic Systems. Science 318:417-420, doi:10.1126/science.1148050
Berman ESF, Levin NE, Landais A, Li S, Owano T (2013) Measurement of $\delta^{18}O$, $\delta^{17}O$, and ^{17}O-excess in Water by Off-Axis Integrated Cavity Output Spectroscopy and Isotope Ratio Mass Spectrometry. Anal Chem 85:10392-10398, doi:10.1021/ac402366t
Bertini I, Gray HB, Lippard SJ, Valentine JS (1994) Bioinorganic Chemistry. University Science Books, Mill Valley, CA
Bigeleisen J (1949) The Relative Reaction Velocities of Isotopic Molecules. J Chem Phys 17:675-678, doi:10.1063/1.1747368
Bigeleisen J, Goeppert-Mayer M (1947) Calculation of equilibrium constants for isotopic exchange reactions. J Chem Phys 15:261-267
Bigeleisen J, Wolfsberg M (1958) Theoretical and experimental aspects of isotope effects in chemical kinetics. Adv Chem Phys 1:15-76

Bindeman IN, Zakharov DO, Palandri J, Greber ND, Dauphas N, Retallack GJ, Hofmann A, Lackey JS, Bekker A (2018) Rapid emergence of subaerial landmasses and onset of a modern hydrologic cycle 2.5 billion years ago. Nature 557:545-548, doi:10.1038/s41586-018-0131-1
Blanchard M, Balan E, Schauble Edwin A (2017) Equilibrium Fractionation of Non-traditional Isotopes: a Molecular Modeling Perspective. Reviews in Mineralogy and Geochemistry 81:27-63, doi:10.2138/rmg.2017.82.2
Bottinga Y (1968) Calculation of fractionation factors for carbon and oxygen isotopic exchange in the system calcite-carbon dioxide-water. J Phys Chem 72:800-808, doi:10.1021/j100849a008
Bourg IC, Sposito G (2008) Isotopic fractionation of noble gases by diffusion in liquid water: Molecular dynamics simulations and hydrologic applications. Geochim Cosmochim Acta 72:2237-2247, doi:10.1016/j.gca.2008.02.012
Bourg IC, Richter FM, Christensen JN, Sposito G (2010) Isotopic mass dependence of metal cation diffusion coefficients in liquid water. Geochim Cosmochim Acta 74:2249-2256, doi:http://dx.doi.org/10.1016/j.gca.2010.01.024
Boys SF, Bernardi F (1970) The calculation of small molecular interactions by the differences of separate total energies. Some procedures with reduced errors. Mol Phys 19:553-566, doi:10.1080/00268977000101561
Buhks E, Bixon M, Jortner J (1981a) Deuterium isotope effects on outer-sphere electron-transfer reactions. J Phys Chem 85:3763-3766, doi:10.1021/j150625a011
Buhks E, Bixon M, Jortner J, Navon G (1981b) Quantum effects on the rates of electron-transfer reactions. J Phys Chem 85:3759-3762, doi:10.1021/j150625a010
Cao X, Liu Y (2011) Equilibrium mass-dependent fractionation relationships for triple oxygen isotopes. Geochim Cosmochim Acta 75:7345-7445
Casado M, Cauquoin A, Landais A, Israel D, Orsi A, Pangui E, Landsberg J, Kerstel E, Prie F, Doussin J-F (2016) Experimental determination and theoretical framework of kinetic fractionation at the water vapour–ice interface at low temperature. Geochim Cosmochim Acta 174:54-69, doi:https://doi.org/10.1016/j.gca.2015.11.009
Celotta RJ, Bennett RA, Hall JL, Siegel MW, Levine J (1972) Molecular Photodetachment Spectrometry. II. The Electron Affinity of O_2 and the Structure of O_2^-. Phys Rev A 6:631-642, doi:10.1103/PhysRevA.6.631
Chacko T, Mayeda TK, Clayton RN, Goldsmith JR (1991) Oxygen and carbon isotope fractionations between CO2 and calcite. Geochim Cosmochim Acta 55:2867-2882, doi:https://doi.org/10.1016/0016-7037(91)90452-B
Clayton RN (2002) Self-shielding in the solar nebula. Nature 415:860-861, doi:10.1038/415860b
Clayton RN, Grossman L, Mayeda TK (1973) A Component of Primitive Nuclear Composition in Carbonaceous Meteorites. Science 182:485-488
Crockford PW, Hayles JA, Bao H, Planavsky NJ, Bekker A, Fralick PW, Halverson GP, Bui TH, Peng Y, Wing BA (2018) Triple oxygen isotope evidence for limited mid-Proterozoic primary productivity. Nature 559:613-616, doi:10.1038/s41586-018-0349-y
Dauphas N, Schauble E, A. (2016) Mass Fractionation Laws, Mass-Independent Effects, and Isotopic Anomalies. Annu Rev Earth Planet Sci 44:709-783, doi:10.1146/annurev-earth-060115-012157
De Vault D, Chance B (1966) Studies of Photosynthesis Using a Pulsed Laser: I. Temperature Dependence of Cytochrome Oxidation Rate in Chromatium. Evidence for Tunneling. Biophys J 6:825-847, doi:10.1016/S0006-3495(66)86698-5
Dieke GH, Babcock HD (1927) The Structure of the Atmospheric Absorption Bands of Oxygen. Proc Natl Acad Sci U S A 13:670-678, doi:10.1073/pnas.13.9.670
Ditchfield R, Hehre WJ, Pople JA (1971) Self-Consistent Molecular-Orbital Methods. IX. An Extended Gaussian-Type Basis for Molecular-Orbital Studies of Organic Molecules. J Chem Phys 54:724-728, doi:10.1063/1.1674902
Dole M (1935) The relative atomic weight of oxygen in water and air. J Am Chem Soc 57:273
Dole M, Jenks G (1944) Isotopic composition of photosynthetic oxygen. Science 100:409

Dole M, Hawkings RC, Barker HA (1947) Bacterial Fractionation of Oxygen Isotopes. J Am Chem Soc 69:226-228
Dove MT, Winkler B, Leslie M, Harris MJ, Salje EKH (1992) A new interatomic potential model for calcite: Applications to lattice dynamics studies, phase transition, and isotope fractionation. Am Mineral 77:244-250
Downs RT, Hall-Wallace M (2003) The American Mineralogist crystal structure database. Am Mineral 88:247-250
Dunning TJ (1989) Gaussian basis sets for use in correlated molecular calculations. I. The atoms boron through neon and hydrogen. J Chem Phys 90:1007-1023
Eiler J, Cartigny P, Hofmann AE, Piasecki A (2013) Non-canonical mass laws in equilibrium isotopic fractionations: Evidence from the vapor pressure isotope effect of SF_6. Geochim Cosmochim Acta 107:205-219, doi:https://doi.org/10.1016/j.gca.2012.12.048
Eiler JM (2007) "Clumped-isotope" geochemistry -- The study of naturally-occurring, multiply-substituted isotopologues. Earth Planet Sci Lett 262:309-327
Eiler JM, Schauble E (2004) $^{18}O^{13}C^{16}O$ in the Earth's atmosphere. Geochim Cosmochim Acta 68:4767-4777
Elcombe MM, Pryor AW (1970) The lattice dynamics of calcium fluoride. Journal of Physics C: Solid State Physics 3:492-499, doi:10.1088/0022-3719/3/3/002
Elcombe MM, Hulston JR (1975) Calculation on sulphur isotope fractionation between sphalerite and galena using lattice dynamics. Earth Planet Sci Lett 28:172-180, doi:https://doi.org/10.1016/0012-821X(75)90224-1
Epstein S, Mayeda T (1953) Variation of O^{18} content of waters from natural sources. Geochim Cosmochim Acta 4:213-224, doi:https://doi.org/10.1016/0016-7037(53)90051-9
Evans MG, Polanyi M (1935) Some applications of the transition state method to the calculation of reaction velocities, especially in solution. Trans Faraday Soc 31:875-894, doi:10.1039/TF9353100875
Eyring H (1935) The Activated Complex in Chemical Reactions. J Chem Phys 3:107-115, doi:doi:http://dx.doi.org/10.1063/1.1749604
Farquhar J, Savarino J, Airieau S, Thiemens MH (2001) Observation of wavelength-sensitive mass-independent sulfur isotope effects during SO_2 photolysis: Implications for the early atmosphere. Journal of Geophysical Research: Planets 106:32829-32839, doi:10.1029/2000JE001437
Frisch MJ, Trucks GW, Schlegel HB*, et al.* (2016) Gaussian 16 Rev. B.01. In Book Gaussian 16 Rev. B.01. Editor, (ed)^(eds), Wallingford, CT
Furche F, Ahlrichs R, Hättig C, Klopper W, Sierka M, Weigend F (2014) Turbomole. WIREs Computational Molecular Science 4:91-100, doi:10.1002/wcms.1162
Gao YQ, Marcus RA (2001) Strange and Unconventional Isotope Effects in Ozone Formation. Science 293:259-263
Giannozzi P, Andreussi O, Brumme T*, et al.* (2017) Advanced capabilities for materials modelling with Quantum ESPRESSO. J Phys: Condens Matter 29:465901, doi:10.1088/1361-648x/aa8f79
Giauque WF, Johnston HL (1929a) An Isotope of Oxygen of Mass 17 in the Earth's Atmosphere. Nature 123:831-831, doi:10.1038/123831a0
Giauque WF, Johnston HL (1929b) An Isotope of Oxygen, Mass 18. Nature 123:318-318, doi:10.1038/123318c0
Gibbons JA, Sharp ZD, Atudorei V (2017) Oxygen Isotope Analyses of Biogenic Carbonate to Reconstruct Early Triassic Ocean Oxygen Isotopic Values and Temperatures. American Geophysical Union Fall Meeting Abstracts:PP14A-04
Grimme S (2006) Semiempirical hybrid density functional with perturbative second-order correlation. J Chem Phys 124:034108, doi:10.1063/1.2148954
Guo W, Zhou C (2019) Triple oxygen isotope fractionation in the DIC-H_2O-CO_2 system: A numerical framework and its implications. Geochim Cosmochim Acta 246:541-564, doi:https://doi.org/10.1016/j.gca.2018.11.018

Guo W, Mosenfelder JL, Goddard III WA, Eiler JM (2009) Isotopic fractionations associated with phosphoric acid digestion of carbonate minerals: Insights from first-principles theoretical modeling and clumped isotope measurements Geochim Cosmochim Acta 73:7203-7225, doi:10.1016/j.gca.2009.05.071
Hariharan PC, Pople JA (1973) The influence of polarization functions on molecular orbital hydrogenation energies. Theor Chim Acta 28:213-222, doi:10.1007/BF00533485
Hathorn BC, Marcus RA (1999) An intramolecular theory of the mass-independent isotope effect for ozone. I. J Chem Phys 111:4087-4100
Hathorn BC, Marcus RA (2000) An intramolecular theory of the mass-independent isotope effect for ozone. II. Numerical implementation at low pressures using a loose transition state. J Chem Phys 113:9497-9509
Hayles J, Gao C, Cao X, Liu Y, Bao H (2018) Theoretical Calibration of the Triple Oxygen Isotope Thermometer. Geochim Cosmochim Acta 235:237-245, doi:https://doi.org/10.1016/j.gca.2018.05.032
Hayles JA, Cao X, Bao H (2017) The statistical mechanical basis of the triple isotope fractionation relationship. Geochem Persp Let 3:1-11, doi:http://dx.doi.org/10.7185/geochemlet.1701
Hayles JA, Yeung LY, Homann M, A. B, Jiang H, Shen B, Lee C-TA (2019) Three Billion Year Secular Evolution of the Triple Oxygen Isotope Composition of Marine Chert.Submitted, doi:10.31223/osf.io/n2p5q
He B, Olack G, Colman A (2012) Pressure baseline correction and high precision CO_2 clumped-isotope (Δ_{47}) measurements in bellows and micro-volume modes. Rapid Commun Mass Spectrom 26:2837-2853
He Y, Bao H (2019) Predicting High-Dimensional Isotope Relationships from Diagnostic Fractionation Factors in Systems with Diffusional Mass Transfer. ACS Earth and Space Chemistry 3:120-128, doi:10.1021/acsearthspacechem.8b00149
Hehre WJ, Ditchfield R, Pople JA (1972) Self—Consistent Molecular Orbital Methods. XII. Further Extensions of Gaussian—Type Basis Sets for Use in Molecular Orbital Studies of Organic Molecules. J Chem Phys 56:2257-2261, doi:10.1063/1.1677527
Helman Y, Barkan E, Eisenstadt D, Luz B, Kaplan A (2005) Fractionation of the Three Stable Oxygen Isotopes by Oxygen-Producing and Oxygen-Consuming Reactions in Photosynthetic Organisms. Plant Physiol 138:2292-2298
Hendricks MB, Bender ML, Barnett BA, Strutton P, Chavez FP (2005) Triple oxygen isotope composition of dissolved O_2 in the equatorial Pacific: A tracer of mixing, production, and respiration. J Geophys Res 110:C12021, doi:10.1029/2004jc002735
Hermida-Ramón JM, Graña AM (2007) Blue-shifting hydrogen bond in the benzene–benzene and benzene–naphthalene complexes. J Comput Chem 28:540-546, doi:10.1002/jcc.20568
Hermida-Ramón JM, Karlström G, Nelander B (2003) On the influence of the basis set superposition error on calculated vibrational frequencies. Theo Chem Acc 110:190-195, doi:10.1007/s00214-003-0471-1
Herwartz D, Pack A, Friedrichs B, Bischoff A (2014) Identification of the giant impactor Theia in lunar rocks. Science 344:1146-1150, doi:10.1126/science.1251117
Hofmann AE, Bourg IC, DePaolo DJ (2012a) Ion desolvation as a mechanism for kinetic isotope fractionation in aqueous systems. Proc Natl Acad Sci U S A 109:18689-18694, doi:10.1073/pnas.1208184109
Hofmann MEG, Horváth B, Pack A (2012b) Triple oxygen isotope equilibrium fractionation between carbon dioxide and water. Earth Planet Sci Lett 319-320:159-164
Hopfield JJ (1974) Electron Transfer Between Biological Molecules by Thermally Activated Tunneling. Proc Natl Acad Sci U S A 71:3640-3644, doi:10.1073/pnas.71.9.3640
Horita J, Wesolowski DJ (1994) Liquid-vapor fractionation of oxygen and hydrogen isotopes of water from the freezing to the critical temperature. Geochim Cosmochim Acta 58:3425-3437, doi:https://doi.org/10.1016/0016-7037(94)90096-5

Huber KP, Herzberg G (1979) Constants of diatomic molecules. Van Nostrand Reinhold Company, New York, NY
Jensen F (2013) Atomic orbital basis sets. WIREs Computational Molecular Science 3:273-295, doi:10.1002/wcms.1123
Jensen F (2017) Introduction to Computational Chemistry. John Wiley & Sons, Ltd., Hoboken, NJ
Juranek LW, Quay PD (2013) Using Triple Isotopes of Dissolved Oxygen to Evaluate Global Marine Productivity. Annu Rev Mar Sci 5:503-524
Kashinski DO, Chase GM, Nelson RG, Di Nallo OE, Scales AN, VanderLey DL, Byrd EFC (2017) Harmonic Vibrational Frequencies: Approximate Global Scaling Factors for TPSS, M06, and M11 Functional Families Using Several Common Basis Sets. J Phys Chem A 121:2265-2273, doi:10.1021/acs.jpca.6b12147
Kesharwani MK, Brauer B, Martin JML (2015) Frequency and Zero-Point Vibrational Energy Scale Factors for Double-Hybrid Density Functionals (and Other Selected Methods): Can Anharmonic Force Fields Be Avoided? J Phys Chem A 119:1701-1714, doi:10.1021/jp508422u
Kieffer SW (1982) Thermodynamics and lattice vibrations of minerals: 5. Applications to phase equilibria, isotopic fractionation, and high-pressure thermodynamic properties. Rev Geophys 20:827-849, doi:10.1029/RG020i004p00827
Kim S-T, O'Neil JR (1997) Equilibrium and nonequilibrium oxygen isotope effects in synthetic carbonates. Geochim Cosmochim Acta 61:3461-3475, doi:https://doi.org/10.1016/S0016-7037(97)00169-5
Kim S-T, Mucci A, Taylor BE (2007) Phosphoric acid fractionation factors for calcite and aragonite between 25 and 75 °C: Revisited. Chem Geol 246:135-146, doi:https://doi.org/10.1016/j.chemgeo.2007.08.005
Knox M, Quay PD, Wilbur D (1992) Kinetic isotope fractionation during air-water gas transfer of O_2, N_2, CH_4, and H_2. J Geophys Res 97:20,335-320,343
Kobko N, Dannenberg JJ (2001) Effect of Basis Set Superposition Error (BSSE) upon ab Initio Calculations of Organic Transition States. J Phys Chem A 105:1944-1950, doi:10.1021/jp001970b
Kohl I, Bao H (2011) Triple-oxygen-isotope determination of molecular oxygen incorporation in sulfate produced during abiotic pyrite oxidation (pH=2–11). Geochim Cosmochim Acta 75:1785-1798, doi:https://doi.org/10.1016/j.gca.2011.01.003
Kohn MJ (1996) Predicting animal $\delta^{18}O$: Accounting for diet and physiological adaptation. Geochim Cosmochim Acta 60:4811-4829, doi:https://doi.org/10.1016/S0016-7037(96)00240-2
Kotaka M, Okamoto M, Bigeleisen J (1992) Anomalous mass effects in isotopic exchange equilibria. J Am Chem Soc 114:6436-6445, doi:10.1021/ja00042a022
Kresse G, Furthmüller J (1996) Efficient iterative schemes for ab initio total-energy calculations using a plane-wave basis set. Phys Rev B 54:11169-11186, doi:10.1103/PhysRevB.54.11169
Kuriyavar SI, Vetrivel R, Hegde SG, Ramaswamy AV, Chakrabarty D, Mahapatra S (2000) Insights into the formation of hydroxyl ions in calcium carbonate: temperature dependent FTIR and molecular modelling studies. J Mater Chem 10:1835-1840, doi:10.1039/B001837F
Lane GA, Dole M (1956) Fractionation of oxygen isotopes during respiration. Science 123:574-576
Laskar AH, Mahata S, Bhattacharya SK, Liang M-C (2019) Triple Oxygen and Clumped Isotope Compositions of CO2 in the Middle Troposphere. Earth and Space Science 6:1205-1219, doi:10.1029/2019ea000573
Lee C, Yang W, Parr RG (1988) Development of the Colle-Salvetti correlation-energy formula into a functional of the electron density. Phys Rev B 37:785-789, doi:10.1103/PhysRevB.37.785
Levien L, Prewitt CT, Weidner DJ (1980) Structure and elastic properties of quartz at pressure. Am Mineral 65:920-930
Levin NE, Raub TD, Dauphas N, Eiler JM (2014) Triple oxygen isotope variations in sedimentary rocks. Geochim Cosmochim Acta 139:173-189, doi:https://doi.org/10.1016/j.gca.2014.04.034

Li B, Yeung LY, Hu H, Ash JL (2019) Kinetic and equilibrium fractionation of O_2 isotopologues during air-water gas transfer and implications for tracing biological oxygen cycling in the ocean. Mar Chem 210:61-71, doi:10.1016/j.marchem.2019.02.006
Li X, Liu Y (2015) A theoretical model of isotopic fractionation by thermal diffusion and its implementation on silicate melts. Geochim Cosmochim Acta 154:18-27, doi:https://doi.org/10.1016/j.gca.2015.01.019
Liljestrand FL, Knoll AH, Tosca NJ, Cohen PA, Macdonald FA, Peng Y, Johnston DT (2020) The triple oxygen isotope composition of Precambrian chert. Earth Planet Sci Lett 537:116167, doi:https://doi.org/10.1016/j.epsl.2020.116167
Liu Q, Tossell JA, Liu Y (2010) On the proper use of the Bigeleisen–Mayer equation and corrections to it in the calculation of isotopic fractionation equilibrium constants. Geochim Cosmochim Acta 74:6965-6983, doi:https://doi.org/10.1016/j.gca.2010.09.014
Luz B, Barkan E (2000) Assessment of Oceanic Productivity with the Triple-Isotope Composition of Dissolved Oxygen. Science 288:2028-2031
Luz B, Barkan E (2005) The isotopic ratios $^{17}O/^{16}O$ and $^{18}O/^{16}O$ in molecular oxygen and their significance in biogeochemistry. Geochim Cosmochim Acta 69:1099-1110
Luz B, Barkan E (2010) Variations of 17O/16O and 18O/16O in meteoric waters. Geochim Cosmochim Acta 74:6276-6286, doi:https://doi.org/10.1016/j.gca.2010.08.016
Luz B, Barkan E (2011) The isotopic composition of atmospheric oxygen. Global Biogeochem Cycles 25:GB3001
Luz B, Barkan E, Severinghaus JP (2014) 5.14 - The Stable Isotopic Composition of Atmospheric O2. *In*: Treatise on Geochemistry (Second Edition). Holland HD, Turekian KK, (eds). Elsevier, Oxford, p 363-383
Luz B, Barkan E, Bender ML, Thiemens MH, Boering KA (1999) Triple-isotope composition of atmospheric oxygen as a tracer of biosphere productivity. Nature 400:547-550
Magyar PM, Orphan VJ, Eiler JM (2016) Measurement of rare isotopologues of nitrous oxide by high-resolution multi-collector mass spectrometry. Rapid Commun Mass Spectrom 30:1923-1940, doi:10.1002/rcm.7671
Mahata S, Bhattacharya SK, Wang C-H, Liang M-C (2013) Oxygen Isotope Exchange between O2 and CO2 over Hot Platinum: An Innovative Technique for Measuring Δ17O in CO2. Anal Chem 85:6894-6901, doi:10.1021/ac4011777
Marcus RA (1952) Unimolecular Dissociations and Free Radical Recombination Reactions. J Chem Phys 20:359-364, doi:10.1063/1.1700424
Marcus RA (2004) Mass-independent isotope effect in the earliest processed solids in the solar system: A possible chemical mechanism. J Chem Phys 121:8201-8211, doi:10.1063/1.1803507
Mardirossian N, Head-Gordon M (2017) Thirty years of density functional theory in computational chemistry: an overview and extensive assessment of 200 density functionals. Mol Phys 115:2315-2372, doi:10.1080/00268976.2017.1333644
Marin-Carbonne J, Chaussidon M, Robert F (2012) Micrometer-scale chemical and isotopic criteria (O and Si) on the origin and history of Precambrian cherts: Implications for paleo-temperature reconstructions. Geochim Cosmochim Acta 92:129-147, doi:https://doi.org/10.1016/j.gca.2012.05.040
Mauersberger K (1981) Measurement of heavy ozone in the stratosphere. Geophys Res Lett 8:935-937
McCrea JM (1950) On the Isotopic Chemistry of Carbonates and a Paleotemperature Scale. J Chem Phys 18:849-857, doi:10.1063/1.1747785
Medvedev MG, Bushmarinov IS, Sun J, Perdew JP, Lyssenko KA (2017) Density functional theory is straying from the path toward the exact functional. Science 355:49-52, doi:10.1126/science.aah5975
Miller MF (2002) Isotopic fractionation and the quantification of ^{17}O anomalies in the oxygen three-isotope system: an appraisal and geochemical significance. Geochim Cosmochim Acta 66:1881-1889
Moran D, Simmonett AC, Leach FE, Allen WD, Schleyer PvR, Schaefer HF (2006) Popular Theoretical Methods Predict Benzene and Arenes To Be Nonplanar. J Am Chem Soc 128:9342-9343, doi:10.1021/ja0630285

Mukherjee A, Smirnov VV, Lanci MP, Brown DE, Shepard EM, Dooley DM, Roth JP (2008) Inner-Sphere Mechanism for Molecular Oxygen Reduction Catalyzed by Copper Amine Oxidases. J Am Chem Soc 130:9459-9473, doi:10.1021/ja801378f
Müller IA, Violay MES, Storck J-C, Fernandez A, van Dijk J, Madonna C, Bernasconi SM (2017) Clumped isotope fractionation during phosphoric acid digestion of carbonates at 70°C. Chem Geol 449:1-14, doi:https://doi.org/10.1016/j.chemgeo.2016.11.030
Mulliken RS (1928) Interpretation of the Atmospheric Oxygen Bands; Electronic Levels of the Oxygen Molecule. Nature 122:505-505, doi:10.1038/122505a0
Murray ST, Arienzo MM, Swart PK (2016) Determining the Δ47 acid fractionation in dolomites. Geochim Cosmochim Acta 174:42-53, doi:https://doi.org/10.1016/j.gca.2015.10.029
Nicholson D, Stanley RHR, Doney SC (2014) The triple oxygen isotope tracer of primary productivity in a dynamic ocean model. Global Biogeochem Cycles 28:doi: 10.1002/2013GB004704
Nier AO (1947) A Mass Spectrometer for Isotope and Gas Analysis. Rev Sci Instrum 18:398-411
NIST Mass Spectrometry Data Center WEW, director (2020) Infrared spectra. *In*: NIST Chemistry WebBook, NIST Standard Reference Database Number 69. Linstrom PJ, Mallard WG, (eds). National Institute of Standards and Technology, Gaithersburg, MD
O'Leary MH (1981) Carbon isotope fractionation in plants. Phytochemistry 20:553-567, doi:https://doi.org/10.1016/0031-9422(81)85134-5
Pack A, Herwartz D (2014a) The triple oxygen isotope composition of the Earth mantle and understanding $\Delta^{17}O$ variations in terrestrial rocks and minerals. Earth Planet Sci Lett 390:138-145, doi:https://doi.org/10.1016/j.epsl.2014.01.017
Pack A, Herwartz D (2014b) The triple oxygen isotope composition of the Earth mantle and understanding variations in terrestrial rocks and minerals. Earth Planet Sci Lett 390:138-145, doi:http://dx.doi.org/10.1016/j.epsl.2014.01.017
Pack A, Gehler A, Süssenberger A (2013) Exploring the usability of isotopically anomalous oxygen in bones and teeth as paleo-CO2-barometer. Geochim Cosmochim Acta 102:306-317, doi:https://doi.org/10.1016/j.gca.2012.10.017
Pack A, Tanaka R, Hering M, Sengupta S, Peters S, Nakamura E (2016) The oxygen isotope composition of San Carlos olivine on the VSMOW2-SLAP2 scale. Rapid Commun Mass Spectrom 30:1495-1504
Pack A, Höweling A, Hezel DC, Stefanak MT, Beck A-K, Peters STM, Sengupta S, Herwartz D, Folco L (2017) Tracing the oxygen isotopic composition of the upper Earth's atmosphere using cosmic spherules. Nat Commun 8:15702
Paier J, Marsman M, Kresse G (2007) Why does the B3LYP hybrid functional fail for metals? J Chem Phys 127:024103, doi:10.1063/1.2747249
Passey BH, Hu H, Ji H, Montanari S, Li S, Henkes GA, Levin NE (2014) Triple oxygen isotopes in biogenic and sedimentary carbonates. Geochim Cosmochim Acta 141:1-25, doi:10.1016/j.gca.2014.06.006
Peng C, Calvin JA, Pavošević F, Zhang J, Valeev EF (2016) Massively Parallel Implementation of Explicitly Correlated Coupled-Cluster Singles and Doubles Using TiledArray Framework. J Phys Chem A 120:10231-10244, doi:10.1021/acs.jpca.6b10150
Perdew JP, Zunger A (1981) Self-interaction correction to density-functional approximations for many-electron systems. Phys Rev B 23:5048-5079, doi:10.1103/PhysRevB.23.5048
Perdew JP, Schmidt K (2001) Jacob's ladder of density functional approximations for the exchange-correlation energy. *In*: Density Functional Theory and Its Application to Materials. Vol 577. Doren VV, Alsenoy CV, Geerlings P, (eds). American Institute of Physics, Melville, NY
Perdew JP, Burke K, Ernzerhof M (1996) Generalized Gradient Approximation Made Simple. Phys Rev Lett 77:3865-3868, doi:10.1103/PhysRevLett.77.3865
Perdew JP, Ruzsinszky A, Csonka GI, Constantin LA, Sun J (2009) Workhorse Semilocal Density Functional for Condensed Matter Physics and Quantum Chemistry. Phys Rev Lett 103:026403, doi:10.1103/PhysRevLett.103.026403

Petersen SV, Defliese WF, Saenger C*, et al.* (2019) Effects of Improved 17O Correction on Interlaboratory Agreement in Clumped Isotope Calibrations, Estimates of Mineral-Specific Offsets, and Temperature Dependence of Acid Digestion Fractionation. Geochem Geophys Geosy 20:3495-3519, doi:10.1029/2018gc008127
Peverati R, Truhlar DG (2011) Improving the Accuracy of Hybrid Meta-GGA Density Functionals by Range Separation. The Journal of Physical Chemistry Letters 2:2810-2817, doi:10.1021/jz201170d
Peverati R, Truhlar DG (2012) M11-L: A Local Density Functional That Provides Improved Accuracy for Electronic Structure Calculations in Chemistry and Physics. The Journal of Physical Chemistry Letters 3:117-124, doi:10.1021/jz201525m
Peverati R, Truhlar DG (2014) Quest for a universal density functional: the accuracy of density functionals across a broad spectrum of databases in chemistry and physics. Philosophical Transactions of the Royal Society A: Mathematical, Physical and Engineering Sciences 372:20120476, doi:doi:10.1098/rsta.2012.0476
Piasecki A, Sessions A, Peterson B, Eiler J (2016) Prediction of equilibrium distributions of isotopologues for methane, ethane and propane using density functional theory. Geochim Cosmochim Acta 190:1-12, doi:https://doi.org/10.1016/j.gca.2016.06.003
Piasecki A, Sessions A, Lawson M, Ferreira AA, Santos Neto EV, Ellis GS, Lewan MD, Eiler JM (2018) Position-specific 13C distributions within propane from experiments and natural gas samples. Geochim Cosmochim Acta 220:110-124, doi:https://doi.org/10.1016/j.gca.2017.09.042
Prokhorov I, Kluge T, Janssen C (2019) Laser Absorption Spectroscopy of Rare and Doubly Substituted Carbon Dioxide Isotopologues. Anal Chem 91:15491-15499, doi:10.1021/acs.analchem.9b03316
Redlich O (1935) Eine allgemeine Beziehung zwischen den Schwingungsfrequenzen isotoper Molekeln. 28B:371, doi:https://doi.org/10.1515/zpch-1935-2834
Richet P, Bottinga Y, Javoy M (1977) A review of hydrogen, carbon, nitrogen, oxygen, sulphur, and chlorine stable isotope fractionation among gaseous molecules. Annu Rev Earth Planet Sci 5:65-110
Richter FM, Mendybaev RA, Christensen JN, Hutcheon ID, Williams RW, Sturchio NC, Beloso AD (2006) Kinetic isotopic fractionation during diffusion of ionic species in water. Geochim Cosmochim Acta 70:277-289, doi:https://doi.org/10.1016/j.gca.2005.09.016
Röckmann T, Brenninkmeijer CAM, Saueressig G, Bergamaschi P, Crowley JN, Fischer H, Crutzen PJ (1998) Mass-Independent Oxygen Isotope Fractionation in Atmospheric CO as a Result of the Reaction CO + OH. Science 281:544-546
Roth JP, Wincek R, Nodet G, Edmondson DE, McIntire WS, Klinman JP (2004) Oxygen Isotope Effects on Electron Transfer to O2 Probed Using Chemically Modified Flavins Bound to Glucose Oxidase. J Am Chem Soc 126:15120-15131, doi:10.1021/ja047050e
Rustad JR, Nelmes SL, Jackson VE, Dixon DA (2008) Quantum-Chemical Calculations of Carbon-Isotope Fractionation in $CO2_{(g)}$, Aqueous Carbonate Species, and Carbonate Minerals. J Phys Chem A 112:542-555, doi:10.1021/jp076103m
Rustad JR, Casey WH, Yin Q-Z, Bylaska EJ, Felmy AR, Bogatko SA, Jackson VE, Dixon DA (2010) Isotopic fractionation of $Mg^{2+(aq)}$, $Ca^{2+(aq)}$, and $Fe^{2+(aq)}$ with carbonate minerals. Geochim Cosmochim Acta 74:6301-6323, doi:https://doi.org/10.1016/j.gca.2010.08.018
Schauble EA (2004) Applying Stable Isotope Fractionation Theory to New Systems. Reviews in Mineralogy and Geochemistry 55:65-111, doi:10.2138/gsrmg.55.1.65
Schauble EA, Ghosh P, Eiler JM (2006a) Preferential formation of $^{13}C–^{18}O$ bonds in carbonate minerals, estimated using first-principles lattice dynamics. Geochim Cosmochim Acta 70:2510-2529, doi:https://doi.org/10.1016/j.gca.2006.02.011
Schauble EA, Ghosh P, Eiler JM (2006b) Preferential formation of $^{13}C–^{18}O$ bonds in carbonate minerals, estimated using first-principles lattice dynamics Geochim Cosmochim Acta 70:2510-2529, doi:10.1016/j.gca.2006.02.011
Schinke R, Grebenshchikov SY, Ivanov MV, Fleurat-Lessard P (2006) Dynamical Studies of the Ozone Isotope Effect: A Status Report. Annu Rev Phys Chem 57:625-661

Schmidt MW, Baldridge KK, Boatz JA, *et al.* (1993) General atomic and molecular electronic structure system. J Comput Chem 14:1347-1363, doi:10.1002/jcc.540141112
Schoenemann SW, Steig EJ (2016) Seasonal and spatial variations of $^{17}O_{excess}$ and d_{excess} in Antarctic precipitation: Insights from an intermediate complexity isotope model. J Geophys Res-Atmos 121:11,215-211,247, doi:10.1002/2016jd025117
Schoenemann SW, Schauer AJ, Steig EJ (2013) Measurement of SLAP2 and GISP $\delta^{17}O$ and proposed VSMOW-SLAP normalization for $\delta^{17}O$ and $^{17}O_{excess}$. Rapid Commun Mass Spectrom 27:582-590, doi:10.1002/rcm.6990
Schwerdtfeger P (2011) The Pseudopotential Approximation in Electronic Structure Theory. ChemPhysChem 12:3143-3155, doi:10.1002/cphc.201100387
Seltzer AM, Ng J, Severinghaus JP (2019) Precise determination of Ar, Kr and Xe isotopic fractionation due to diffusion and dissolution in fresh water. Earth Planet Sci Lett 514:156-165, doi:https://doi.org/10.1016/j.epsl.2019.03.008
Sengupta S, Pack A (2018) Triple oxygen isotope mass balance for the Earth's oceans with application to Archean cherts. Chem Geol 495:18-26, doi:https://doi.org/10.1016/j.chemgeo.2018.07.012
Shao Y, Gan Z, Epifanovsky E, *et al.* (2015) Advances in molecular quantum chemistry contained in the Q-Chem 4 program package. Mol Phys 113:184-215, doi:10.1080/00268976.2014.952696
Sharp ZD (1990) A laser-based microanalytical method for the in situ determination of oxygen isotope ratios of silicates and oxides. Geochim Cosmochim Acta 54:1353-1357, doi:http://dx.doi.org/10.1016/0016-7037(90)90160-M
Sharp ZD, Wostbrock JAG, Pack A (2018) Mass-dependent triple oxygen isotope variations in terrestrial materials. Geochem Persp Let 7:27-31, doi:http://dx.doi.org/10.7185/geochemlet.1815
Sharp ZD, Gibbons JA, Maltsev O, Atudorei V, Pack A, Sengupta S, Shock EL, Knauth LP (2016) A calibration of the triple oxygen isotope fractionation in the SiO_2–H_2O system and applications to natural samples. Geochim Cosmochim Acta 186:105-119
Skaron S, Wolfsberg M (1980) Anomalies in the fractionation by chemical equilibrium of 18O/16O relative to 17O/16O. J Chem Phys 72:6810-6811, doi:10.1063/1.439177
Staroverov VN, Scuseria GE, Tao J, Perdew JP (2003) Comparative assessment of a new nonempirical density functional: Molecules and hydrogen-bonded complexes. J Chem Phys 119:12129-12137, doi:10.1063/1.1626543
Stefurak EJT, Fischer WW, Lowe DR (2015) Texture-specific Si isotope variations in Barberton Greenstone Belt cherts record low temperature fractionations in early Archean seawater. Geochim Cosmochim Acta 150:26-52, doi:https://doi.org/10.1016/j.gca.2014.11.014
Steig EJ, Gkinis V, Schauer AJ, Schoenemann SW, Samek K, Hoffnagle J, Dennis KJ, Tan SM (2014) Calibrated high-precision ^{17}O-excess measurements using cavity ring-down spectroscopy with laser-current-tuned cavity resonance. Atmos Meas Tech 7:2421-2435, doi:10.5194/amt-7-2421-2014
Stipp SLS, Eggleston CM, Nielsen BS (1994) Calcite surface structure observed at microtopographic and molecular scales with atomic force microscopy (AFM). Geochim Cosmochim Acta 58:3023-3033, doi:https://doi.org/10.1016/0016-7037(94)90176-7
Stolper DA, Fischer WW, Bender ML (2018) Effects of temperature and carbon source on the isotopic fractionations associated with O_2 respiration for $^{17}O/^{16}O$ and $^{18}O/^{16}O$ ratios in *E. coli*. Geochim Cosmochim Acta 240:152-172, doi:https://doi.org/10.1016/j.gca.2018.07.039
Su NQ, Zhu Z, Xu X (2018) Doubly hybrid density functionals that correctly describe both density and energy for atoms. Proc Natl Acad Sci U S A 115:2287-2292, doi:10.1073/pnas.1713047115
Sun T, Bao H (2011) Thermal-gradient-induced non-mass-dependent isotope fractionation. Rapid Commun Mass Spectrom 25:765-773, doi:10.1002/rcm.4912
Sutherland KM, Wostbrock JAG, Hansel CM, Sharp ZD, Hein JR, Wankel SD (2020) Ferromanganese crusts as recorders of marine dissolved oxygen. Earth Planet Sci Lett 533:116057, doi:https://doi.org/10.1016/j.epsl.2019.116057

Swart PK, Murray ST, Staudigel PT, Hodell DA (2019) Oxygen Isotopic Exchange Between CO_2 and Phosphoric Acid: Implications for the Measurement of Clumped Isotopes in Carbonates. Geochem Geophys Geosy 20:3730-3750, doi:10.1029/2019gc008209
Tanaka R, Nakamura E (2012) Determination of ^{17}O-excess of terrestrial silicate/oxide minerals with respect to Vienna Standard Mean Ocean Water (VSMOW). Rapid Commun Mass Spectrom 27:285-297, doi:10.1002/rcm.6453
Tao J, Perdew JP, Staroverov VN, Scuseria GE (2003) Climbing the Density Functional Ladder: Nonempirical Meta--Generalized Gradient Approximation Designed for Molecules and Solids. Phys Rev Lett 91:146401, doi:10.1103/PhysRevLett.91.146401
Thiemens MH (2006) History and Applications of Mass-Independent Isotope Effects. Annu Rev Earth Planet Sci 34:217-262
Thiemens MH, Heidenreich JE (1983) The Mass-Independent Fractionation of Oxygen: A Novel Isotope Effect and its Possible Cosmochemical Implications. Science 219:1073-1075
Tyroller L, Brennwald MS, Mächler L, Livingstone DM, Kipfer R (2014) Fractionation of Ne and Ar isotopes by molecular diffusion in water. Geochim Cosmochim Acta 136:60-66, doi:https://doi.org/10.1016/j.gca.2014.03.040
Tyroller L, Brennwald MS, Busemann H, Maden C, Baur H, Kipfer R (2018) Negligible fractionation of Kr and Xe isotopes by molecular diffusion in water. Earth Planet Sci Lett 492:73-78, doi:https://doi.org/10.1016/j.epsl.2018.03.047
Urey HC (1947) The thermodynamic properties of isotopic substances. J Chem Soc 47:562-581
Valiev M, Bylaska EJ, Govind N*, et al.* (2010) NWChem: A comprehensive and scalable open-source solution for large scale molecular simulations. Comput Phys Commun 181:1477-1489, doi:https://doi.org/10.1016/j.cpc.2010.04.018
Voarintsoa NRG, Barkan E, Bergel S, Vieten R, Affek HP (2020) Triple oxygen isotope fractionation between CaCO3 and H2O in inorganically precipitated calcite and aragonite. Chem Geol 539:119500, doi:https://doi.org/10.1016/j.chemgeo.2020.119500
Vogiatzis KD, Ma D, Olsen J, Gagliardi L, Jong WAd (2017) Pushing configuration-interaction to the limit: Towards massively parallel MCSCF calculations. J Chem Phys 147:184111, doi:10.1063/1.4989858
Waldeck AR, Cowie BR, Bertran E, Wing BA, Halevy I, Johnston DT (2019) Deciphering the atmospheric signal in marine sulfate oxygen isotope composition. Earth Planet Sci Lett 522:12-19, doi:https://doi.org/10.1016/j.epsl.2019.06.013
Wang Z, Schauble EA, Eiler JM (2004) Equilibrium thermodynamics of multiply substituted isotopologues of molecular gases. Geochim Cosmochim Acta 68:4779-4797
Watkins JM, DePaolo DJ, Watson EB (2017) Kinetic Fractionation of Non-Traditional Stable Isotopes by Diffusion and Crystal Growth Reactions. Reviews in Mineralogy and Geochemistry 82:85-125, doi:10.2138/rmg.2017.82.4
Watkins JM, Hunt JD, Ryerson FJ, DePaolo DJ (2014) The influence of temperature, pH, and growth rate on the $\delta^{18}O$ composition of inorganically precipitated calcite. Earth Planet Sci Lett 404:332-343, doi:https://doi.org/10.1016/j.epsl.2014.07.036
Weigend F, Ahlrichs R (2005) Balanced basis sets of split valence, triple zeta valence and quadruple zeta valence quality for H to Rn: Design and assessment of accuracy. Phys Chem Chem Phys 7:3297-3305, doi:10.1039/B508541A
Wigner E (1932) On the quantum correction for thermodynamic equilibrium. Phys Rev 40:749
Winta CJ, Gewinner S, Schöllkopf W, Wolf M, Paarmann A (2018) Second-harmonic phonon spectroscopy of $\ensuremath{\alpha}$-quartz. Phys Rev B 97:094108, doi:10.1103/PhysRevB.97.094108
Witte J, Neaton JB, Head-Gordon M (2016) Push it to the limit: Characterizing the convergence of common sequences of basis sets for intermolecular interactions as described by density functional theory. J Chem Phys 144:194306, doi:10.1063/1.4949536

Wostbrock JAG, Cano EJ, Sharp ZD (2020) An internally consistent triple oxygen isotope calibration of standards for silicates, carbonates and air relative to VSMOW2 and SLAP2. Chem Geol 533:119432, doi:https://doi.org/10.1016/j.chemgeo.2019.119432

Wostbrock JAG, Sharp ZD, Sanchez-Yanez C, Reich M, van den Heuvel DB, Benning LG (2018) Calibration and application of silica-water triple oxygen isotope thermometry to geothermal systems in Iceland and Chile. Geochim Cosmochim Acta 234:84-97, doi:https://doi.org/10.1016/j.gca.2018.05.007

Xu X, Alecu IM, Truhlar DG (2011) How Well Can Modern Density Functionals Predict Internuclear Distances at Transition States? J Chem Theory Comput 7:1667-1676, doi:10.1021/ct2001057

Yeung LY, Young ED, Schauble EA (2012) Measurements of $^{18}O^{18}O$ and $^{17}O^{18}O$ in the atmosphere and the influence of isotope-exchange reactions. J Geophys Res 117:D18306, doi:10.1029/2012JD017992

Yeung LY, Hayles JA, Hu H, Ash JL, Sun T (2018) Scale distortion from pressure baselines as a source of inaccuracy in triple-isotope measurements. Rapid Commun Mass Spectrom, doi:10.1002/rcm.8247

Yeung LY, Li S, Kohl IE, Haslun JA, Ostrom NE, Hu H, Fischer TP, Schauble EA, Young ED (2017) Extreme enrichment in atmospheric $^{15}N^{15}N$. Sci Adv 3, doi:10.1126/sciadv.aao6741

Young ED, Galy A, Nagahara H (2002) Kinetic and equilibrium mass-dependent isotope fractionation laws in nature and ther geochemical and cosmochemical significance. Geochim Cosmochim Acta 66:1095-1104

Young ED, Yeung LY, Kohl IE (2014) On the $\Delta^{17}O$ Budget of Atmospheric O_2. Geochim Cosmochim Acta 135:102-125, doi:doi: 10.1016/j.gca.2014.03.026

Young ED, Kohl IE, Warren PH, Rubie DC, Jacobson SA, Morbidelli A (2016) Oxygen isotopic evidence for vigorous mixing during the Moon-forming giant impact. Science 351:493-496, doi:10.1126/science.aad0525

Zhang S, Liu Q, Tang M, Liu Y (2020) Molecular-Level Mechanism of Phosphoric Acid Digestion of Carbonates and Recalibration of the ^{13}C–^{18}O Clumped Isotope Thermometer. ACS Earth and Space Chemistry 4:420-433, doi:10.1021/acsearthspacechem.9b00307